Molecular composition and volatility of multi-generation products formed from isoprene oxidation by nitrate radical

Rongrong Wu[1,2], Luc Vereecken[1], Epameinondas Tsiligiannis[3], Sungah Kang[1], Sascha R. Albrecht[1,a], Luisa Hantschke[1], Defeng Zhao[4], Anna Novelli[1], Hendrik Fuchs[1], Ralf Tillmann[1], Thorsten Hohaus[1], Philip T.M. Carlsson[1], Justin Shenolikar[5], François Bernard[6], John N. Crowley[5], Juliane L. Fry[7], Bellamy Brownwood[7], Joel A. Thornton[8], Steven S. Brown[9,10], Astrid Kiendler-Scharr[1], Andreas Wahner[1], Mattias Hallquist[3], Thomas F. Mentel[1*]

[1]Institute of Energy and Climate Research, Troposphere (IEK-8), Forschungszentrum Jülich GmbH, 52428 Jülich, Germany
[2]College of Environmental Sciences and Engineering, State Key Joint Laboratory of Environmental Simulation and Pollution Control, Peking University, 100871, Beijing, China
[3]Department of Chemistry and Molecular Biology, University of Gothenburg, 41296, Gothenburg, Sweden
[4]Department of Atmospheric and Oceanic Sciences & Institute of Atmospheric Sciences, Fudan University, 200438, Shanghai, China
[5]Atmospheric Chemistry Department, Max Planck Institut für Chemie, 55128 Mainz, Germany
[6]Institut de Combustion, Aérothermique, Réactivité et Environnement (ICARE), UPR CNRS, 45071 Orléans, France
[7]Department of Chemistry, Reed College, Portland, OR 97202, USA
[8]Department of Atmospheric Sciences, University of Washington, Seattle, WA 98195, USA
[9]NOAA Chemical Sciences Laboratory, Boulder, CO 80305, USA
[10]Department of Chemistry, University of Colorado, Boulder, CO 80309, USA
[a]present address: SOLIDpower GmbH, 52525 Heinsberg, Germany

[*]*Correspondence to*: Thomas F. Mentel (t.mentel@fz-juelich.de)

Abstract

Isoprene oxidation by nitrate radical (NO_3) is a potentially important source of secondary organic aerosol (SOA). It is suggested that the second or later-generation products are the more substantial contributors to SOA. However, there are few studies investigating the multi-generation chemistry of isoprene-NO_3 reaction, and information about the volatility of different isoprene nitrates, which is essential to evaluate their potential to form SOA and determine their atmospheric fate, is rare. In this work, we studied the reaction between isoprene and NO_3 in the SAPHIR chamber (Jülich) under near atmospheric conditions. Various oxidation products were measured by a high-resolution time-of-flight chemical ionization mass spectrometer using Br^- as the reagent ion. Most of the products detected are organic nitrates, and they are grouped into monomers (C_4- and C_5-products), and dimers (C_{10}-products) with 1–3 nitrate groups according to their chemical composition. Most of the observed products match expected termination products observed in previous studies, but some compounds such as monomers and dimers with three nitrogen atoms were rarely reported in the literature as gas-phase products from isoprene oxidation by NO_3. Possible formation mechanisms for these compounds are proposed. The multi-generation chemistry of isoprene and NO_3 is characterized by taking advantages of the time behavior of different products. In addition, the vapor pressures of diverse isoprene nitrates are calculated by different parametrization methods. An estimation of the vapor pressure is also derived from their condensation behavior. According to our results, isoprene monomers belong to intermediate volatility or semi-volatile organic compounds and thus have little effect on SOA formation. In contrast, the dimers are expected to have low or

extremely low volatility, indicating that they are potentially substantial contributors to SOA. However, the monomers constitute 80% of the total explained signals on average, while the dimers contribute less than 2%, suggesting that the contribution of isoprene NO_3 oxidation to SOA by condensation should be low under atmospheric conditions. We expect a SOA mass yield of about 5 % from the wall loss and dilution corrected mass concentrations, assuming that all of the isoprene dimers in the low- or extremely low-volatility organic compound (LVOC or ELVOC) range will condense completely.

1. Introduction

Atmospheric submicron aerosols have an adverse effect on air quality, human health and climate (Jimenez et al., 2009; Pöschl, 2005). Secondary organic aerosol (SOA), which is formed from oxidation of volatile organic compounds (VOC) followed by gas-to-particle partitioning, comprise a large fraction (20-90%) of the submicron aerosol mass (Jimenez et al., 2009; Zhang et al., 2007). It is confirmed that a significant proportion of SOA arises from biogenic VOC (BVOC) oxidation (Hallquist et al., 2009; Spracklen et al., 2011).

Isoprene is globally the most abundant non-methane volatile organic compound originating from vegetation, with emissions estimated to be 440-660 Tg yr^{-1}(Guenther et al., 2012). Due to its high abundance, as well as its high reactivity with atmospheric oxidants, isoprene plays a significant role in tropospheric chemistry, and its chemistry affects the global aerosol burden and distribution (Carlton et al., 2009; Fry et al., 2018; Ng et al., 2008, 2017; Surratt et al., 2010), although its SOA yield is much lower than those of monoterpenes and sesquiterpenes (Friedman and Farmer, 2018; Kim et al., 2015; Marais et al., 2016; , McFiggans, et al. 2019; Mutzel et al., 2016; Ng et al., 2007, 2008; Surratt et al., 2010; Thornton et al., 2020). Recent model simulations suggested the isoprene-derived SOA production is 56.7 Tg C yr^{-1}, contributing up to 41% of global SOA (Stadtler et al., 2018). Observations in southeastern United States suggested that isoprene-derived SOA makes up 17- 48% of total organic aerosol (Hu et al., 2015; Kim et al., 2015; Marais et al., 2016). As a consequence, it is essential to fully characterize the potential of isoprene to form condensable products and its contribution to SOA formation (Carlton et al., 2009).

Although the majority of isoprene emissions is emitted by plants and is light-dependent, isoprene emitted in the day can persist in the boundary layer after sunset, and its mixing ratio can remain as high as several ppb (Brown et al., 2009; Starn et al., 1998; Stroud et al., 2002; Warneke et al., 2004). During the daytime, isoprene is primarily oxidized by the hydroxyl radical (OH) and somewhat by ozone (O_3), but its main oxidizers shift to nitrate radical (NO_3) and O_3 in the nighttime (Wennberg et al., 2018). Due to the higher reactivity of NO_3 with isoprene (k_{NO_3} = 6.5 ×10^{-13} cm^3 $molecules^{-1}s^{-1}$ and k_{O_3} = 1.28 ×10^{-17} cm^3 $molecules^{-1}s^{-1}$ at 298 K, respectively, IUPAC), a considerable fraction of the residual isoprene would be oxidized by NO_3 at night, and therefore nocturnal nitrate radical chemistry is typically thought to be of significant importance for isoprene, especially in regions where sufficient nitrogen oxides are available (Brown et al., 2009; Fry et al., 2018; Ng et al., 2017; Wennberg et al., 2018). Although reaction with NO_3 only represents ~ 5-6% of isoprene loss, it accounts for a large proportion of organic nitrates derived from isoprene oxidation (~ 40-50%) (Wennberg et al., 2018). Therefore, reaction of isoprene with NO_3 is a potential source of SOA. In addition, it is found from both laboratory and chamber experiments that the SOA yield of isoprene from NO_3 oxidation is higher than that from OH or O_3 oxidation, which is typically less than 5% (Carlton et al., 2009; Dommen et al., 2009; Kleindienst et al., 2007; Kroll et al., 2006). For example, Ng et al. (2008) concluded the isoprene SOA yield from NO_3 was in the range of 4.3% to 23.8%, depending on RO_2 fate (higher SOA yield when the experiments were dominated by RO_2+RO_2 rather than RO_2+NO_3 reaction). Rollins et al. (2009) also observed a high SOA yield from isoprene (14%) when both of its double bonds were oxidized by NO_3. In an aircraft study in the southeastern United States, Fry et al. (2018) derived an isoprene-NO_3 SOA yield as large as 27% on average under high NO_x conditions, although their mass yield estimation was indirect, and based on a molar yield determination of 9 ± 5%. In light of the relatively high SOA yield from NO_3 oxidation, even though only a minor fraction of isoprene is oxidized by NO_3, the SOA formed at nighttime would still probably be comparable to that produced at daytime (Brown et al., 2009; Fry et al., 2018).

However, isoprene-NO_3 chemistry (Wennberg et al. 2018, Vereecken et al. 2021) has received less attention than the extensively studied OH- or O_3-initiated oxidation (Barber et al., 2018; Novelli et al., 2020; Peeters et al., 2014; Wang et al., 2018; Wennberg et al., 2018; Whalley et al., 2012). It has been recognized that later-generation oxidation of isoprene by NO_3 makes more significant contribution to SOA formation (Carlton et al., 2009; Fry et al., 2018; Rollins et al., 2009). Nevertheless, although the importance of multi-generation NO_3 oxidation of isoprene to SOA formation has been recognized, few studies extended the investigation beyond the first-generation oxidation, and details of isoprene-NO_3 multi-generation chemistry are still lacking.

Organic compounds, especially highly oxygenated organic molecules (HOM) that have low or extremely low volatility, contribute significantly to SOA formation by condensation, or even form new particles (Bianchi et al., 2019; Ehn et al., 2014; Kirkby et al., 2016, Tröstl et al., 2016). Previous studies have confirmed that low-volatility products from isoprene-NO_3 reaction are the major precursors to SOA (Ng et al., 2008; Rollins et al., 2009; Schwantes et al., 2019). Here the low-volatility compounds refer to gas phase products that allow fractions to exist in particle-phase, and may include the groups of organic compounds with intermediate volatility (IVOC, $300<C^*<3\times10^6$ μg m^{-3}), semi-volatility (SVOC, $0.3<C^*<300$ μg m^{-3}), low volatility (LVOC, $3\times10^{-5}<C^*<0.3$ μg m^{-3}) and extremely low volatility (ELVOC, $C^*<3\times10^{-5}$ μg m^{-3}) as proposed by Donahue et al. (2012). In general, SVOC, LVOC and ELVOC can contribute to the SOA formation (Jimenez et al., 2009). In order to evaluate the potential of oxygenated products to form SOA, information about their vapor pressures is essential. However, due to the high degree of functionalization, low or extremely low volatility, as well as uncertainties in quantification and molecular structures, it is challenging to determine the exact vapor pressure of highly oxidized products. Detailed information on the volatilities of different generation products is lacking, which impedes the assessment of their contribution to SOA formation.

In this work, we present the results of chamber experiments on isoprene oxidation by NO_3 under near atmospheric conditions, where NO_3 was produced in situ by O_3 reaction with NO_2. Subsequent characteristics of multi-generation chemistry of isoprene with NO_3 are investigated. By examining the time evolution of various gas-phase products, we propose possible reaction mechanisms that help to get the possible functionalization of the products. Saturation vapor pressures of the major gas-phase products observed by HR-ToF-CIMS are predicted by using different parameterization methods that are widely-used or state-of-the-art in literature. In addition, we estimate the vapor pressure derived from equilibrium partitioning coefficient according to the condensation behavior of different products in experiments with and without seed aerosols. Based on these results, the volatility of the major oxidation products stemming from isoprene-NO_3 reaction and their potential to form SOA are evaluated.

2. Experimental and methods

2.1 Atmospheric simulation chamber SAPHIR

All the data presented here were measured in the atmospheric simulation chamber SAPHIR (**S**imulation of **A**tmospheric **PH**otochemical **I**n a large **R**eaction Chamber) at Forschungszentrum Jülich, Germany, which is designed to investigate the oxidation processes of both biogenic and anthropogenic trace gases and formation of secondary particles and pollutants under near atmospheric conditions. The SAPHIR chamber is a double-walled Teflon (FEP) cylinder with a volume of 270 m^3 (5 meters in diameter and 18 meters in length). The large volume-to-surface ratio (1 m) allows experiments to be conducted under natural conditions and reduces interference from the chamber walls. The chamber is equipped with a shutter system which can be opened to admit sunlight for photochemical experiments or closed to mimic nighttime conditions. There are two fans inside the chamber to ensure good mixing of trace gases (within 2 minutes). The chamber is filled with synthetic air made from mixing of ultrapure nitrogen and oxygen (Linde, purity ≥ 99.99990%) and is slightly over-pressured (~ 35 Pa) to prevent intrusion of outside air into the chamber. Due to small leakage (~ 7 m^3 h^{-1}) and gas consumption by instrument sampling, a replenishment flow is provided by a flow control, which leads to a dilution rate of 4%–7% per hour. A more detailed description of the chamber set-up and its characterization can be found elsewhere (Rohrer et al., 2005).

2.2 Experiment description

A series of experiments investigating the oxidation of isoprene by NO_3 were conducted in the SAPHIR chamber in August 2018 (ISOPNO$_3$ campaign) under different chemical conditions. In this work, we primarily focus on an experiment conducted on 08 August 2018 that examined the fast oxidation of isoprene by NO_3 (up to ~ 130 pptv) without seed aerosols. The experiment was performed under dry (RH < 5%) and dark condition, and employed injections of O_3 and NO_2 as source of NO_3, where O_3 was generated by a silent discharge ozoniser (O3onia), and high-purity NO_2 was introduced from a gas bottle (Linde, purity >99%).

Before the experiment, the chamber was flushed overnight with a total amount of ~ 1800 m^3 synthetic air to minimize any remaining contamination. At the beginning of the experiment, the chamber air was slightly humidified (RH< 0.1%) by flushing water vapor from boiling Milli-Q® water into the chamber. Thereafter, O_3 and NO_2 were added to the chamber in succession, and their concentrations in the chamber after injection were approximately 100 and 25 ppbv, respectively, as shown in Fig. 1. After that, ~10 ppbv of isoprene was injected using a GC syringe, initiating the reaction with NO_3. The period between the first and second injection is defined as "step I", as so on for the other three periods. The second injection was done when isoprene from the first injection was almost completely consumed, to reach concentrations of O_3, NO_2, and isoprene in the chamber of ~100, 30, and 10 ppbv, respectively. About 1.5 hours later, the chemistry was further accelerated by a third injection of precursors, and accordingly the concentrations of O_3, NO_2, and isoprene reached ~ 100, 25, and 10 ppbv, respectively. Two hours later, the fourth addition was made and the concentrations of O_3 and NO_2 increased to approximately 115 ppbv and 30 ppbv, respectively, aiming to promote further oxidation of early generation products. In total the system was kept running for about 7.5 h. Calculation from measurements of isoprene, O_3, OH, NO_3 and dilution indicates that NO_3 contributed for more than 90% of the chemical losses of isoprene, as shown in Fig. S1, with reaction with O_3 being a minor pathway in our system. The reaction of isoprene with OH was not considered as OH concentration was below the detection limit of the instrument in this study (Fig. S2). Thus, losses due to reaction with OH could not be quantified from the measurement, but have been determined to contribute about 10% of the isoprene losses according to a recently published modelling work based on the same campaign, with the contribution of the NO_3 reaction accounting for up to 80% accordingly (Vereecken et al., 2021).

A complementary experiment was conducted on 14 August 2018 under similar conditions but with seed aerosols. Approximately 60 μg m^{-3} of ammonium sulfate aerosol was added at the beginning of the experiment. Thereafter, approximate 100 and 20 ppbv of O_3 and NO_2 were introduced to the chamber to produce NO_3, followed by addition of ~10 ppbv of isoprene in about 30 minutes later (see Fig. S3). Another 6 ppbv of NO_2 and 10 ppbv of isoprene were added about one hour later to accelerate the reaction. At the last injection, only O_3 (~ 50 ppbv) and NO_2 (~ 7 ppbv) were added, similar as for the experiment without seeds. The experiment lasted for about 8 h. The results were used to investigate the condensation behavior of various gas-phase products from isoprene oxidation, aiming to estimate equilibrium partitioning coefficients and vapor pressures.

2.3 Instrumentation

A high-resolution time-of-flight chemical ionization mass spectrometer (HR-ToF-CIMS, Aerodyne Research Inc., hereafter CIMS) was used to continuously measure the gas-phase products from isoprene oxidation by NO_3. The ToF-MS was operated in 'V' mode with the mass resolution power between 3000–4000 Th/Th. In order to reduce the losses of HO_2 radicals and HOM on the tubing, a customized inlet (Albrecht et al., 2019) was directly connected to the chamber. The CIMS was operated in negative ion mode using Br^- as the reagent ion, which is selective to polar species such as acids, hydroxy or nitrooxy carbonyls, as well as HO_2 radicals (Albrecht et al., 2019; Ng et al., 2008; Rissanen et al., 2019; Riva et al., 2019).

Bromide ions were generated by passing a mixture of 10 standard cubic centimeters per minute of 0.4% CF_3Br in nitrogen and 2 standard liter per minute nitrogen through a 370 MBq ^{210}Po source (Type P-2021-5000, NDR Static Control LLC, USA), resulting in ~10^5 ion counts per second (Albrecht et al., 2019). In our system, on average, about 190 ions were identified for each mass spectrum on average, most of which were detected as adducts with Br^-, while some acidic compounds (~ 7% of the total) like nitric acid (HNO_3), glycolic acid ($C_2H_4O_3$), and malonic acid ($C_3H_4O_4$) were also detected as deprotonated ions. In addition, there were some ions (~ 10% of the total) identified as adducts with NO_3^-. The isotope distribution of ^{79}Br and ^{81}Br is approximately 1:1, therefore two signals appear at m/z = MW+79 and m/z = MW+81 with MW being the molecular mass of the molecule that is detected as cluster with Br^-. In this work, we will use Thomson (Th) as the unit for mass-to-charge (m/z), and the m/z of molecules discussed in following include the mass contribution from Br^- (m/z 79) if there is no other annotation.

In order to have an indicator of the CIMS performance, perfluoropentanoic acid (PFPA, $C_5F_9HO_2$) was used as an internal standard. For m/z calibration, five isolated peaks were used, including Br^- (m/z 79), H_2OBr^- (m/z 97), HNO_3Br^- (m/z 142), $C_5F_9O_2^-$ (m/z 263), and $C_5F_9HO_2Br^-$ (m/z 343), covering the mass range of dominant products. The averaged accuracies of all five calibrated masses were below 5 ppm over the whole measurement period. However, due to the low signal intensity, the PFPA cluster ($C_{10}F_{18}O_4H^-$, m/z 527) was not suited for mass calibration, and there were no other suitable masses with sufficient intensity and high accuracy that could be used to calibrate the higher mass range. Therefore, peak fitting in the mass range between 300 to 500+ Th might have higher uncertainties. The CIMS was optimized to gain a maximum signal of $[HO_2*Br]^-$ isotopes, which are weakly bounded clusters. This was achieved by adjusting step by step the electrostatic field in the transfer stage to minimize fragmentation. During the campaign, the settings of CIMS were kept unchanged to keep a similar performance. However, the signal of reagent ion Br^- decreased by about 65% (from ~ 100, 000 to 34, 000 counts s^{-1}) over the campaign duration of four weeks. In order to minimize the effect of drift in performance, we used the normalized (by the sum of the total ion counts) signals for analysis. The sensitivity for total carbon was calculated by determining the slope of wall-loss corrected total carbon signals detected by CIMS (only the identified peaks were considered) versus isoprene consumed. As illustrated in Fig. S4a, the CIMS sensitivities were roughly identical in two experiments (0.026 ± 0.002 norm. count s^{-1} $ppbv^{-1}$ on 08 August, and 0.022 ± 0.001 norm. count s^{-1} $ppbv^{-1}$ on 14 August), indicating that different experimental conditions over two days had an insignificant impact on CIMS sensitivity for total carbon and thus the data from these days are comparable. In addition, an inter-comparison of measurements by Br^- CIMS and I^- CIMS were made. As shown in Fig. S4b, the measurements of $C_5H_6N_2O_8$ from the two instruments are well linearly correlated with each other at the early oxidation stages. However, the correlation coefficients of measurements from two instruments deviated from experiment to experiment. This is probably related to different experimental conditions, which might lead to different chemical processes and thus formation of isomers. Since CIMS with different reagent ions might have different sensitivities to isomers, and may be selective for different compounds, the correlation coefficients of measurements from Br^- and I^- CIMS may differ from day to day. Moreover, the Br^- CIMS was not tuned during the campaign while the I^- CIMS was optimized from time to time. In general, the performance of Br^- CIMS was stable and the data taken by it are reliable.

The mass spectra data were processed using the software "Tofware" embedded in Igor as provided by Aerodyne Research Inc. (https://www.tofwerk.com/software/tofware/?cn-reloaded=1). Peaks detected in the mass spectra could be isolated and identified according to their exact mass, and molecular formulas and the corresponding intensities were obtained by high-resolution peak fitting. Due to a lack of authentic standards for the products, it is difficult to quantitatively determine their individual absolute concentrations, but we have calculated the bulk sensitivity for organonitrates by using the sum of organic nitrate signals from Br^- CIMS divided by measurements of the total alkyl nitrates from a thermal dissociation-cavity ring-down spectrometer during the experiment . The estimated bulk sensitivities for organonitrates are 0.016 ± 0.001 and 0.022 ± 0.001 norm. count s^{-1} $ppbv^{-1}$on 08 August and 14 August, respectively, as shown in Fig. S4c, comparable to the sensitivity for total carbon, but smaller than the sensitivity for salicylic acid determined by an independent calibration (163 norm. count μg^{-1} on average as shown in Fig. S4d, equal to 0.07 norm. count s^{-1} $ppbv^{-1}$). The bulk sensitivity for organonitrates enables estimation of the absolute concentrations of products assuming that they have identical sensitivity. In this study we use the normalized signals instead of absolute concentrations for analysis. This is sufficient here because our analysis focuses on the time evolution of signals and the relative changes of intensities, so the absolute concentrations are not necessarily needed. The sensitivity derived above is only used to convert the signals of dimers to concentrations in order to estimate the SOA yield.

Isoprene was measured by a Vocus proton transfer reaction time-of-flight mass spectrometer (Aerodyne Research Inc., hereafter Vocus), which has a higher mass resolving power (nominal 10000 Th/Th) and less inlet wall losses and sampling delays compared to traditional PTR-MS (Krechmer et al., 2018). The mixing ratio of O_3 was monitored by an UV absorption instrument, and that of NO_2 was monitored by a chemiluminescence instrument and a custom-built cavity ring-down spectrometer (CRDS). The concentrations of NO_3 and N_2O_5 were detected by two custom-built CRDS instruments (Dubé et al., 2006; Sobanski et al., 2016). In addition, temperature and pressure inside the chamber were monitored by an ultra-sonic anemometer and a pressure sensor, respectively. The relative humidity was primarily detected as water mixing ratio by a Picarro CRDS instrument (Crosson, 2008).

The particle number concentrations and their size distributions were measured by a condensation particle counter (TSI 3783, hereafter CPC) and a scan mobility particle sizer (TSI 3081 electrostatic classifier combined with TSI 3025 CPC, hereafter SMPS). The aerosol chemical composition was identified by a high-resolution time of flight aerosol mass spectrometer (HR-ToF-AMS, Aerodyne Research Inc., hereafter AMS). The ionization efficiency of AMS was determined by using the monodisperse aerosol generated from NH_4NO_3 and $(NH_4)_2SO_4$ solutions. The collection efficiency (CE) could be estimated based on the particle mass concentration yielded from AMS and that derived from SMPS. In this study, the average CE value of 0.5 is used for correction.

2.4 Methods to estimate saturation vapor pressure

The pure liquid saturation vapor pressure is a thermodynamic metric relevant for the partitioning equilibrium of organic molecules, which determines their propensity to form SOA (Compernolle et al., 2011; O'Meara et al., 2014; Pankow and Asher, 2008). Due to their complex functionalities and low or extremely low volatility, it is challenging to determine the vapor pressures of highly oxidized molecules. As a result, theoretical and semiempirical methods are usually used for vapor pressure estimation. Commonly used semiempirical methods include composition-activity (CA), group-contribution (GC), and structure-activity (SA) methods. The CA methods are the easiest to use, as they only require information on molecular composition for estimation. They are widely applied in context of the two-dimensional volatility basis set (2D-VBS) (Donahue et al., 2011). For GC methods, the exact functional groups are required to calculate the saturation vapor pressure. The SIMPOL.1 (Pankow and Asher, 2008), the parameterization as described by Nannoolal et al. (2008), and EVAPORATION (Compernolle et al., 2011) are three widely used GC methods. Structure-activity methods can provide more accurate estimates with sophisticated treatments of intramolecular interactions like intramolecular hydrogen-bonding (Bilde et al., 2015). However, detailed molecular properties such as boiling point and evaporation enthalpy are required for estimation, which are generally obtained by complex and time-consuming quantum chemical calculations. Therefore, SA methods are not applied for vapor pressure estimation in this study.

Saturation concentration (C^*, mass based) is related to saturation vapor pressure and can be calculated following Eq. (1) (Donahue et al., 2006). The $\log_{10}(C^*)$ is a metric used in the 2D-VBS method to evaluate the volatility of organic molecules.

$$C_i^* = \frac{M_i 10^6 \zeta_i p_i^\circ}{RT} \quad (1)$$

where R (8.206×10^{-5} m^3 atm K^{-1} mol^{-1}) is the gas constant, T (K) is the temperature, M_i (g mol^{-1}) is the molecular weight of compound i, ζ_i is the activity coefficient of compound i and here is assumed to be 1 (Donahue et al., 2006), p_i° (atm) is the pure liquid saturation vapor pressure at temperature T (298 K).

In this study, different CA methods are applied to calculate the saturation vapor pressures of various oxidation products from isoprene reaction with NO_3. These include parameterizations that were constrained by chamber measurements as proposed by Donahue et al. (2011), Mohr et al. (2019), and Peräkylä et al. (2019). All of these three parameterization methods have included the effect of the presence of nitrate groups on vapor-pressure estimation. Further we test the GC methods proposed by Nannoolal et al. (2008), Pankow and Asher (2008, SIMPOL.1), and Compernolle et al. (2011, EVAPORATION). All the methods used in this study are summarized in Table 1. The calculations of EVAPORATION and the Nannool method were done via the online molecular and multiphase property prediction facility UManSysProp (http://umansysprop.seaes.manchester.ac.uk/tool/vapour_pressure). For the latter the boiling point parameterization method needs to be predefined, and that from Nannoolal et al. (2004) was adopted as recommended by O'Meara et al. (2014). The information about molecular structures needed for the calculation is inferred from mechanistic information, which is described in detail in Sect. 2.5.

In addition, we take advantage of the measurements in this study to calculate the gas-particle equilibrium partitioning coefficient (K) by comparing experiments with and without seed aerosols. The partitioning coefficient K can be converted to saturation concentration C^* by Eq. (2).

$$K_i = \frac{C_{i,p}}{C_{i,g} \times C_{OA}} = \frac{1}{C_i^*} \tag{2}$$

where $C_{i,g}$ and $C_{i,p}$ are the gas- and particle-phase concentrations (μg m^{-3}) of species i, respectively, and C_{OA} is the organic aerosol concentration (μg m^{-3}). In this study, $C_{i,g}$ is signal of species *i* from CIMS in the experiment with seeds, and $C_{i,p}$ is the difference of signals between experiment without and with seeds (under the same isoprene consumption condition). The C_{OA} in the experiment with seeds is in a range of 1-4 μg m^{-3}.

2.5 Pathways to the multifunctional oxidation products

2.5.1 Basic peroxy and alkoxy radical chemistry

As mentioned before, information about molecular structures (at least functional groups) is required to calculate vapor pressures by using GC methods. Although the high-resolution ToF-CIMS allows for determining chemical composition of the detected ions, it is unable to provide information about molecular structures, so that the constitutional or configurational isomers with the same mass cannot be distinguished without additional information. Fortunately, knowledge of detailed chemical formation mechanisms can help inferring the molecular structure information. However, the development of a comprehensive, multi-generational kinetic mechanism for NO_3-initiated oxidation of isoprene is outside the scope of the current paper. Instead, in order to link the observed mass peaks to representative molecular structures, we developed a framework tracing the chemical oxidation mechanisms by taking well-known oxidation steps to predict the most likely isomeric forms of the functionalized products formed in the isoprene oxidation. For this purpose, we rely on the extensive literature on isoprene, alkylperoxy radical, and alkoxy radical chemistry (Atkinson, 2007; Atkinson and Arey, 2003; Bianchi et al., 2019; Crounse et al., 2013; Ehn et al., 2014; Jenkin et al., 2015; Jenkin et al., 2019; Kwan et al., 2012; Mentel et al., 2015; Ng et al., 2008; Noveli et al., 2021; Orlando et al., 2003; Orlando and Tyndall, 2012; Rollins et al., 2009; Schwantes et al., 2015; Vereecken and Francisco, 2012; Vereecken and Peeters, 2009, 2010; Vereecken et al., 2021; Wennberg et al., 2018; Ziemann and Atkinson, 2012). This framework is depicted in the supporting information and will be discussed in more detail in Sect. 2.5.2 and Sect. 2.5.3. They are based on the following main reactivity trends.

Generally, RO_2 radicals can react with other RO_2 and HO_2 radicals. There are three major channels for the reaction between two RO_2 radicals, leading to alkoxy radicals (RO) (Reaction R1a), as well as termination products like alcohols, aldehydes or ketones (Reaction R1b) and accretion products (Reaction R1c). These reactions should take place with the first-generation peroxy radicals, as well as with the higher generation RO_2 radicals formed in the later oxidation steps. Hydroperoxides can be formed from the reaction of RO_2 with HO_2 radicals (Reaction R2a). This reaction can also yield alkoxy radicals (Reaction R2b).

$$RO_2\cdot + R'O_2\cdot \longrightarrow RO\cdot + R'O\cdot + O_2 \quad \text{(R1a)}$$

$$RO_2\cdot + R'O_2\cdot \longrightarrow ROH + R'_{-H}{=}O + O_2 \quad \text{(R1b)}$$

$$RO_2\cdot + R'O_2\cdot \longrightarrow ROOR' + O_2 \quad \text{(R1c)}$$

$$RO_2\cdot + HO_2\cdot \longrightarrow ROOH + O_2 \quad \text{(R2a)}$$

$$RO_2\cdot + HO_2\cdot \longrightarrow RO\cdot + \cdot OH + O_2 \quad \text{(R2b)}$$

In the presence of NO_x, RO_2 radicals can also react with NO and NO_2, leading to the formation of alkoxy radicals (R3a), organic nitrates (R3b), and peroxynitrates (R4) (including peroxyacyl nitrates, PANs, if R = $R'C(O)$–). The channel that results in RO radicals is the major pathway for the reaction of RO_2 radicals with NO (Ziemann and Atkinson, 2012). However, reactions of RO_2 radicals with NO (Reaction R3a and R3b) can be neglected in this study due to the high O_3 concentration, which results in rapid conversion of NO to NO_2. The peroxynitrates formed from the reaction of RO_2 with NO_2 will undergo rapid thermal decomposition under our experimental conditions, with exception of PANs. The reaction of RO_2 with NO_3 radicals mainly forms NO_2 and alkoxy radicals (Reaction R5), which will continue the radical chains (Reaction R7).

$$RO_2\cdot + NO \longrightarrow RO\cdot + NO_2 \quad \text{(R3a)}$$

$$RO_2\cdot + NO \longrightarrow RONO_2 \quad \text{(R3b)}$$

$$RO_2\cdot + NO_2 + M \longleftrightarrow ROONO_2 + M \quad \text{(R4)}$$

$$RO_2\cdot + NO_3 \longrightarrow RO\cdot + NO_2 + O_2 \quad \text{(R5)}$$

In addition to bimolecular reactions, intramolecular rearrangement (H-migration) is a competitive reaction pathway for RO_2 radicals. RO_2 radicals can undergo H-migration to form a hydroperoxy functionality (–OOH) and a radical site that can subsequently recombine with an O_2 molecule, leading to the formation of a new, more oxidized substituted RO_2 (Reaction R6). This process is the so-called “autoxidation” path and has been confirmed as a significantly important way for SOA formation (Crounse et al., 2013; Ehn et al., 2014; Mentel et al., 2015; Praske et al., 2018; Rissanen et al., 2014). The rates of RO_2 H-migration are strongly dependent on the structure of RO_2 radicals, and the most likely routes can be derived based on the structure-activity relationship proposed by Vereecken and Nozière (2020).

$$RO_2\cdot \longrightarrow HOOQ\cdot\,;\quad HOOQ\cdot + O_2 \longrightarrow Q(OOH)O_2\cdot \quad \text{(R6)}$$

The RO radicals formed in in the reaction of RO_2 + RO_2 typically have three accessible pathways, including isomerization by H-migration (Reaction R7a), fragmentation (Reaction R7b) and less important here, reaction with O_2 (Reaction R7c). Like H-migration in RO_2, rearrangement by H-shift in RO radicals leads to the formation of more oxidized RO_2 radicals. Fragmentation leads to smaller carbon chains, and this becomes more important for alkoxy radicals with a higher number of (oxygen-bearing) substituents (Vereecken and Peeters, 2009, 2010).

$$RO\cdot \longrightarrow HOQ\cdot\,;\quad HOQ\cdot + O_2 \longrightarrow R(OH)O_2\cdot \quad \text{(R7a)}$$

$$RO\cdot \longrightarrow R'{=}O + R''\cdot \quad \text{(R7b)}$$

$$RO\cdot + O_2 \longrightarrow R{=}O + HO_2\cdot \quad \text{(R7c)}$$

In addition to the above general reaction pathways, we include a number of other reactions in the framework, such as fragmentation of peroxy radicals, epoxidation of β-OOH alkyl radicals, and unimolecular termination of nitrooxy or hydroperoxyl peroxy radicals. Details can be found in the supporting information.

2.5.2 Formation of first-generation products

Here "first-generation products" refers to the closed-shell compounds from the first attack of NO_3 at the isoprene double bonds, while "second-generation products" follow an addition of NO_3 to the remaining double bond (or any other oxidation reaction) of a first-generation product. Addition of a NO_3 radical to one of isoprene double bonds and subsequent addition of O_2 to the resulting (delocalized) radical sites leads to the formation of nitrooxy alkylperoxy radicals (INO_2, $C_5H_8NO_3$). Since isoprene contains two double bonds, NO_3 can attack any of the four positions on the conjugated carbon bonds, resulting in eight possible INO_2 isomers (including six constitutional and two conformational isomers), as shown in Scheme S1. However, both theoretical and experimental studies suggest that the addition occurs preferably at the primary and terminal carbons, wherein C1 addition seems to be preferred over C4 addition (Schwantes et al., 2015; Suh et al., 2001; Wennberg et al., 2018). As the GC methods have limited or no ability to distinguish between positional isomers (Kurten et al., 2016), we take exemplarily the products following the C1 addition for the vapor pressure analysis in this study.

The initial peroxy radicals ($C_5H_8NO_3$) can undergo rearrangement by H shift from C–H bonds with subsequent O_2 addition, yielding new –OOH functionalized peroxy radicals (Reaction R6). Repeating this process can lead to the formation of a series of peroxy radicals and termination products with stepwise increasing number of oxygen atoms by 2, as shown in the conceptual scheme Scheme S2. This is the RO_2 autoxidation channel and the molecular formula of peroxy radicals formed via consecutive O_2 additions can be represented as $C_5H_8NO_{(3+2n)}$ ($n \geq 1$, number of autoxidation steps). The autoxidation chain can be terminated when the H-shift occurs at a carbon with an –OOH or $–ONO_2$ group attached, leading to carbonyl formation with OH or NO_2 loss (Anglada et al., 2016; Bianchi et al., 2019; Vereecken, 2008; Vereecken et al., 2004). The closed-shell products formed in these termination steps have the general molecular formula $C_5H_7NO_{(5+2n-1)}$ (OH loss channel) or $C_5H_8O_{(3+2n-2)}$ (NO_2 loss channel).

The $C_5H_8NO_{(3+2n)}$ peroxy radicals can also react with HO_2 radicals to form –OOH functionalized termination products with the general molecular formula $C_5H_9NO_{(3+2n)}$ (Reaction R2a), or yielding the alkoxy radicals $C_5H_8NO_{(3+2n-1)}$ (Reaction R2b). In addition, the $C_5H_8NO_{(3+2n)}$ peroxy radicals can react with other $RO_2^{\cdot}$ radicals (Reaction R1a-R1c). The reaction R1a leads to the formation of alkoxy radicals ($C_5H_8NO_{(3+2n-1)}$) while R1b forms closed-shell products either with a carbonyl group ($C_5H_7NO_{(3+2n-1)}$) or a hydroxyl group ($C_5H_9NO_{(5+2n-1)}$). Alternatively, dimers can be formed following Reaction R1c, which have then two $–ONO_2$ groups and at least 8 oxygen atoms depending on the formula of RO_2 radicals involved, as shown in Table S1.

The alkoxy radicals from reactions R1a and R2b can undergo unimolecular rearrangement by H shift with subsequent O_2 addition, similar to the RO_2 radicals, forming new RO_2 radicals with a –OH group (Reaction R7a). As mentioned above, when the H-shift occurs at a carbon with an –OOH or $–ONO_2$ group attached, the resulting intermediates tend to lose an OH group or NO_2 (Bianchi et al., 2019), yielding the closed-shell carbonyl products with general formulas $C_5H_7NO_{(5+2n-2)}$ or $C_5H_8O_{(3+2n-3)}$ respectively, as shown in the conceptual scheme Scheme S3. The newly-formed RO_2 radicals from alkoxy H-shift channel can follow the peroxy pathways (Reaction R1-R6) like other RO_2 radicals, leading to a diversity of compounds like hydroperoxides

(Reaction R2a, $C_5H_9NO_{(3+2n+1)}$), alcohols (Reaction R1b, $C_5H_9NO_{(3+2n)}$), aldehydes (Reaction R1b, $C_5H_7NO_{(3+2n)}$) as well as accretion products (Reaction R1c, $C_{10}H_{16}N_2O_x$), as depicted in Scheme S3. Alternatively, they can also yield alkoxy radicals again following reactions R1a and R2b and continue so on. Furthermore, the alkoxy radicals can break apart into two fragments according to Reaction R7b.

In general, the alkoxy reaction pathways diversify the parity of the oxygen number of the products from the reaction of isoprene with NO_3, and the compounds formed via these reactions generally have one less or one more oxygen atom compared to those formed from straight peroxy reaction pathways. With help of the mechanistic framework described above, we can infer the functionality of first-generation products. This is exemplified in Scheme S5 and S6 for the major first-generation C_5 products. In addition, the reaction pathways and their corresponding structures of the first-generation C_{10} dimers ($C_{10}H_{16}N_2O_x$) are summarized in Scheme S13.

2.5.3 Formation of second-generation products

Nitrate radicals can oxidize the first-generation products once again at the double bond remaining (k_{NO_3}(298K) ~ 3-11×10^{14} cm^3 $molecule^{-1}$ s^{-1}, Wennberg et al., 2018). This leads eventually to "second-generation" products that contain at least two nitrogen atoms. Addition of NO_3 radical to the remaining double bond of the first-generation products results in the formation of dinitrooxy peroxy radicals. We assume that dinitrooxy peroxy radicals can undergo unimolecular and bimolecular reactions (Reaction R1–R6) in analogy to nitrooxy peroxy radicals, which lead to secondary products containing two or more nitrogen atoms, as summarized in the conceptual scheme Scheme S4.

The reaction of first-generation nitrooxy peroxy radicals with NO_2 can also yield 2N-compounds (Reaction R4), however these 2N-compounds ought to be under first-generation products by definition. Such species are not discussed in detail here but will be covered to catch the diversity of the functionalities for the vapor pressure estimation. With the help of this secondary reaction framework, we can propose functional groups for the major second-generation products. Scheme S8 – S10 depict the detailed (possible) reaction pathways that lead to the formation of detected C_5 dinitrates, as well as their possible structures. Furthermore, the proposed formation mechanism and their structures for C_5 trinitrates are shown in Scheme S12, while those for the second-generation C_{10} dimers ($C_{10}H_{17}N_3O_x$ and $C_{10}H_{18}N_4O_x$) are depicted in Scheme S13.

2.5.4 Formation of fragmentation products

In addition to the multigenerational C_5 and C_{10} products, fragmentation products can be formed from the reaction of isoprene with NO_3. As mentioned above, the alkoxy radicals can undergo C–C bond scission, producing a carbonyl compound and an alkyl fragment (Reaction R7b). As shown in Scheme S7, when the secondary nitrooxy alkoxy radicals from the further oxidation of C_5 carbonyl compounds ($C_5H_8O_2$ and $C_5H_8O_3$ here) undergo unimolecular decomposition, C_4 carbonyl products ($C_4H_7NO_5$ and $C_4H_7NO_6$, respectively) are formed as well as formyl radicals. Since the bond fission can occur at different positions, the generation of more reactive C_2 and C_3 carbonyl compounds are possible. In addition, the C_4 carbonyl compounds are possibly generated through peroxy radical arrangement by 1,4 H-shift and subsequent acyl radical bond scission reactions (see Scheme S7). The C_4 dinitrates can be formed following similar chemistry, as depicted in Scheme S11.

2.5.5 Candidate structures for vapor pressure estimation

Among all gas-phase products detected by CIMS, we selected 32 major representative organonitrates formed from isoprene oxidation by NO_3 radicals. Their structures are rationalized by the corresponding molecular formulas and proposed formation mechanisms in the reaction framework. Table S2 summarizes all the exemplified structures used for vapor pressure estimation. The functional groups covered in the selected structures include nitrate, hydroxyl, ketone, aldehyde, carboxylic acid, peroxide, hydroperoxide, hydroperoxy acid, peroxynitrate, peroxyacyl nitrate and epoxide. The structural information allows calculation of the saturation vapor pressure by GC methods.

3. Results and discussion

3.1 Chemical composition of oxidation products

Figure 2 illustrates the average mass spectra of the whole experiment measured by Br^-CIMS for isoprene-NO_3 reaction. Chemical sum formulas were attributed to most of the detected ions. The gas-phase products were separated into two major groups according to their chemical composition, including monomers comprising C_5 compounds and dimers containing C_{10} compounds. There were also products from decomposition reactions with $C_{<5}$, which were merged into monomers. The monomers and dimers were further classified into five subgroups as follows. Monomers consisting of compounds with one nitrogen atom (hereafter 1N-monomers) and two or three N atoms (2N- or 3N-monomers) mainly accumulate in *m/z* 220–280 Th, *m/z* 300–340 Th and 350–390 Th, respectively, while dimers containing compounds with two N atoms (2N-dimers) and three N atoms (3N-dimers) appear in *m/z* 370–440 Th and 450–520 Th, respectively. As shown in Fig. 2, the signal intensities decrease from 1N-monomers, 2N-monomers, 2N-dimers to 3N-monomers and 3N-dimers. Many of the compounds detected in this work were also observed in previous isoprene-NO_3 systems (Kwan et al., 2012; Ng et al., 2008; Schwantes et al., 2015). In this work, only closed-shell products are considered for analysis.

The 1N-monomer $C_5H_9NO_5$ at *m/z* 242 is the dominant product formed from the NO_3-induced isoprene oxidation in our experiment, followed by the 1N-decomposition product $C_4H_7NO_5$ at *m/z* 228. In addition to $C_5H_9NO_5$, several analogues with molecular formulas $C_5H_7NO_{4\text{-}7}$ and $C_5H_9NO_4$ are in relatively high abundance. $C_5H_{8,10}N_2O_{8,9}$ and $C_5H_9N_3O_{10\text{-}12}$ are the major 2N- and 3N-monomers. Their signal intensities are one to two orders of magnitude lower than those of 1N-monomers. According to the chemical composition, the 1N-monomers are likely to be the first-generation products from NO_3 oxidation of isoprene, while the 2N- and 3N-monomers probably arise from the further oxidation of 1N-monomers by NO_3, which therefore should be second- or later-generation products. As mentioned before, the reaction of nitrooxy alkylperoxy radicals with NO_2 can lead to the formation of peroxynitrates (for the special case peroxyacyl nitrates, PAN-like) containing two N atoms. The peroxynitrates will decompose rapidly under experimental conditions, whereas the PAN-like compounds are more stable (with lifetimes ranging from minutes to weeks at 298K and ambient temperature). Such C_5 PAN-like compounds are isomers of aforementioned 2N-monomers, but ought to be first-generation products. In addition to C_5-2N-monomers, we observe some C_4-2N-monomers with relatively high intensity, such as $C_4H_6N_2O_7$ at *m/z* 273 and $C_4H_8N_2O_8$ at *m/z* 291. It is proposed that such C_4 dinitrates originate from the further oxidation of C_5 carbonyl compounds followed by unimolecular decomposition (Schwantes et al., 2015; Wennberg et al., 2018), as shown in Scheme S11.

2N-Dimers are C_{10} compounds with 8-12 oxygen atoms ($C_{10}H_{16}N_2O_{8-12}$), and their signal intensities are relatively low compared to that of monomers, approximately three orders of magnitude lower. They might be ROOR products from the self or cross reaction of two nitrooxy peroxy radicals (Berndt et al., 2018). 3N-Dimers are molecules consisting of 12–16 oxygen atoms ($C_{10}H_{17}N_3O_{12-16}$). They are probably formed from further oxidation of 2N-dimers or from the cross reaction of a nitrooxy peroxy radical with a dinitrooxy peroxy radicals.

3.2 Multi-generation chemistry

3.2.1 Molecular composition for each step

As mentioned in Sect. 2.2, there were four injections during the experiment on 8 August (denoted as step I, II, III, IV in Fig. 3), wherein in the first three injections all components, O_3, NO_2, and isoprene, were added, while in the last step only O_3 and NO_2 were injected to promote the further oxidation of early-generation products. The extended oxidation time with reinjection of oxidants provides the opportunity to investigate the multi-generation oxidation chemistry of isoprene-NO_3 system. The mass spectra show only slow changes in the concentrations during the last period of each step, indicating weak chemical evolution. Therefore, we use integrated mass spectra over the last 10 minutes of each step for further analysis. Due to the similarity of the integrated mass spectra for step II and step III, the latter is omitted in Fig. 3.

As shown in Fig. 3a, large amounts of 1N-monomers were formed from NO_3 oxidation of isoprene in step I, wherein $C_5H_9NO_5$, $C_5H_9NO_6$, and $C_4H_7NO_5$ are the most abundant compounds in signal. The 2N-monomers, which are expected from further oxidation of 1N-monomers, are much less compared to 1N-monomers, accounting for 5.0% of the total organic signals, with the 3N-monomers even less (0.04%). The low contributions of second-generation products probably results from the relatively high concentration of isoprene in step I, reducing the possibility for further oxidation of first-generation products. These results indicate that the system is dominated by first-generation chemistry at the early stage and therefore the oxidation state of products is low. In addition to monomers, some 2N- and 3N-dimers are observed. They contribute 1.7% and 0.2%, respectively, to the total organic signals, as shown in Fig. 3b. The low signal intensity of dimers probably results from their small yield under our experimental conditions. In this case their contribution to SOA formation might be small. However, a part of the dimers condense onto chamber wall due to their low volatility, so only a smaller portion exists in the gas phase (compare Table S3 and Fig. S5).

In step II, the secondary chemistry was accelerated by further addition of O_3 and NO_2, but the primary chemistry was also maintained by isoprene injection. As a result, more 1N-monomers (e.g. $C_5H_9NO_{4,5,6}$) were formed compared to step I, as well as dimers (e.g., $C_{10}H_{16}N_2O_{8,9,10}$ and $C_{10}H_{17}N_3O_{12,13}$), as shown in Fig. 3a. The signals of 2N-monomers almost double in this period compared to those in step I, and their relative contribution increase from 5.0% to 7.4%. This is attributed to the further oxidation of first-generation products formed in step I. The relative contributions of different chemical groups exhibited in Fig. 3b clearly show that, although NO_3 produced from the second addition of NO_2 and O_3 still primarily reacted with newly-injected isoprene, reaction of NO_3 with the first-generation oxidation products retaining a double bond was inevitable, leading to more second-generation 2N- or 3N-products compared to step I. The visibly increasing fraction of 2N-monomers indicates that the second-generation chemistry started to play a more important role than that in the early stage. In step III, the chemical process proceeded similarly, and thus is not further discussed here.

Due to the favorable conditions for further oxidation, the signals of 1N-monomers (such as $C_5H_9NO_4$, $C_5H_9NO_5$, and $C_5H_9NO_6$), as well as 2N- and 3N-dimers, dropped dramatically in step IV, with their relative contributions decreasing to 58.1%, 0.5%, and 0.15%, respectively. The decrease in signals of dimers is primarily ascribed to lack of isoprene, as there were less peroxy radicals under this condition, and hence less dimers were formed. In addition, their condensation on the wall and dilution also contributed to the decreasing signals. Furthermore, dimers with 2 or 3 nitrogen atoms possess at least one double bond in their molecular structures and can thus be further oxidized under high NO_3 condition to form 4N- or 5N-dimers. However, only few 4N-dimers and no 5N-dimers were detected by CIMS, suggesting that the 4N- and 5N-dimers were either not formed, or if present, with lower absolute concentrations below the detection limit (approximately 5×10^7 and 5×10^5 molecules cm^{-3} for salicylic acid and acetic acid, for an integration time of 60 s). condensed on the wall due to their low volatilities. In contrast, 2N- and 3N-monomers increase significantly, with their relative contributions ascending to 20.0% and 0.29%, respectively. This indicates that 2N- and 3N-monomers might be second- or later-generation products that are formed from the further oxidation of first-generation products. Additionally, unlike the C_5 monomers, the signal of $C_4H_7NO_5$ increased in step IV, indicating that there is a new formation pathway for $C_4H_7NO_5$ under excess NO_3 condition. No double bond can remain in such products, as otherwise they would be oxidized and their signal should decay instead.

In summary, above findings confirm that multi-generation chemistry happened during the NO_3-initiated isoprene oxidation, and that the later generation oxidation was promoted by "excess" NO_3 radicals.

3.2.2 Carbon oxidation state ($\overline{OS_C}$)

The oxidation state of carbon ($\overline{OS_C}$) is defined as the charge a carbon atom takes with assumption that it loses completely all electrons in bonds to more electronegative atoms and vice versa (Kroll et al., 2011). This quantity is a metric for the degree of oxidation and will increase with oxidation. Moreover, $\overline{OS_C}$ together with carbon number can be used to constrain the composition of organic mixtures and provide insights into their evolutions. The carbon oxidation state of a species is determined by the relative abundances and oxidation states of non-carbon atoms in the compound. Since we observed nitrate groups in the products, $\overline{OS_C}$ is defined by Eq. (3). In this study, the group-averaged $\overline{OS_C}$ is the signal-weighted mean average carbon oxidation state of compounds with the same carbon number, and the bulk-averaged $\overline{OS_C}$ is the signal-weighted mean average carbon oxidation state of all detected compounds in the system.

$$\overline{OS_C} = \frac{2 \times n_O - n_H - 5 \times n_N}{n_C} \quad (3)$$

wherein, n_O, n_H, and n_N are the number of the respective atoms in the molecular formula.

Figure 4 shows the distribution of gas-phase products from the isoprene-NO_3 system in the oxidation state versus carbon number (OS_C vs n_C) space. The bulk-averaged $\overline{OS_C}$ is -0.35 in step I, wherein the smaller molecules ($C_{\leqslant 4}$) have higher oxidation states than the larger molecules. The group-averaged oxidation state of C_5 compounds is relatively low ($\overline{OS_{C=5}}$= -0.66), indicating that both of the oxidation and autoxidation degree of isoprene are quite low during this period. This is consistent with the conclusion made previously from mass spectra results that at the early stage isoprene-NO_3 oxidation was dominated by first-generation chemistry.

The system $\overline{\mathrm{OS_C}}$ increases to -0.26 in step II, confirming that first-generation products were further oxidized after the second injection. During this step, the $\overline{\mathrm{OS_C}}$ of most compound groups increase only weakly, except for that of the C_5 compounds. The group-averaged $\overline{\mathrm{OS_C}}$ of C_5 compounds increases to -0.60 in step II, which is the major contributor to the increase of $\overline{\mathrm{OS_C}}$ of the whole system. The increase of $\overline{\mathrm{OS_C}}$ of C_5 compounds is largely attributed to the formation of 2N-monomers expected from further oxidation of existing 1N-products formed in step I. This is confirmed by the detectable increase of 2N- and 3N-monomers in the mass spectra and their higher relative contributions to total signals (see Fig. 3). In addition to C_5 compounds, the $\overline{\mathrm{OS_C}}$ of C_3 and C_6 products increase significantly in step II.

In step IV, the secondary oxidation was largely accelerated by reinjection of O_3 and NO_2, and hence the system oxidation degree increases, with the bulk-averaged $\overline{\mathrm{OS_C}}$ growing substantially to 0.09. Similarly, the significant increase of system $\overline{\mathrm{OS_C}}$ is mainly attributed to the C_5 compounds, with their group-averaged $\overline{\mathrm{OS_C}}$ increasing to -0.31. In addition, the $\overline{\mathrm{OS_C}}$ of C_{10} compounds increased evidently despite their decreasing signals, suggesting C_{10} dimers were further oxidized as well in step IV. It is worth noting that the average carbon number decreases step by step with increasing $\overline{\mathrm{OS_C}}$. This is the case because fewer C_{10} products, but more fragments were formed with the reaction proceeding, as shown in Fig.4 by the decreasing peak areas of larger molecules but converse trend for smaller molecules. One conceivable explanation for the decreasing dimers but increasing fragments with the increasing $\overline{\mathrm{OS_C}}$ is that, with more highly oxidized RO_2 formed under high NO_3 condition, the prevailing fate of RO_2 changes from dimerization to forming alkoxy radicals, which would undergo unimolecular decomposition rapidly, especially when there is a neighboring oxygen-containing functional group (Molteni et al., 2019).

In the oxidation system, the increase in $\overline{OS_C}$ is attributed to the formation of bonds between carbon and oxygen as well as other electronegative atoms, and/ or the breaking of bonds between carbon and hydrogen and other electropositive atoms (Kroll et al., 2011). The $–ONO_2$ group has an oxidation state of -1, which means that addition of a $–ONO_2$ group to isoprene will increase its OS_C by 0.2. According to our estimates, the values of system $\overline{OS_C}$ increased by 1.25 (step I), 0.09 (step II), and 0.35 (step IV), indicating that the increases in $\overline{OS_C}$ are not only due to addition of $–ONO_2$ group(s) but also to other oxygen-containing functionalities. In addition to functionalization, it is possible that other reactions such as fragmentation and oligomerization which can increase or reduce the oxidation state were involved during the reaction.

As mentioned above, the average carbon oxidation state of a mixture of molecules largely depends on its chemical composition. Therefore, for different oxidation systems, their $\overline{OS_C}$ may differ due to different precursors and oxidation conditions. In our study, the $\overline{OS_C}$ of NO_3-initiated isoprene oxidation system increased from -0.35 to 0.09 with further oxidation. For OH- and O_3-initiated systems, the average oxidation state of laboratory-generated isoprene SOA are reported to range from -1.3 to -0.2, as listed in Table S4. It seems that the SOA generated from chloride-initiated oxidation of isoprene is more oxidized compared to other isoprene oxidation systems, for which the $\overline{OS_C}$ can be as high as +1.8 according to limited studies (Wang and Ruiz, 2017). With regard to ambient measurements, the calculated $\overline{OS_C}$ values of organic aerosol and aerosol fractions fell into a wider range between -2 to +2, depending on the site position and the corresponding oxidation environment of that site (Table S4).

In summary, isoprene and its products undergo further oxidation by NO_3, leading to an increase in degree of oxidation of products as the reaction proceeds. The increasing bulk $\overline{OS_C}$ is largely governed by the highly oxidized C_5 compounds. In addition, more fragments but fewer dimers are formed as the $\overline{OS_C}$ increases, which can be probably explained by the change of RO_2 fate from prevailing dimerization to fragmentation through the alkoxy radical channel.

3.2.3 Characteristics of different-generation products

(1) 1N-monomers

To illustrate the multi-generation chemistry involved in the isoprene-NO_3 reaction system, Fig. 5 shows the time evolution of the major gas-phase products. The signal of the most abundant compounds, $C_5H_9NO_5$, increases rapidly as soon as the reaction was initiated, reaching a maximum when its chemical production rate matches its loss rate (including chemical destruction, wall loss, dilution, etc.), and decreases slowly thereafter. Its time behavior in the first three steps is similar. In step IV, however, the injection of O_3 and NO_2 resulted in a strong decay of $C_5H_9NO_5$, owing to the occurrence of further oxidation by NO_3. The time behavior suggests that $C_5H_9NO_5$ signal is dominated by first-generation oxidation products, and the same conclusion can be made for $C_5H_9NO_4$ and $C_5H_9NO_6$. According to the mechanistic framework developed above, the $C_5H_9NO_4$, $C_5H_9NO_5$, and $C_5H_9NO_6$ compounds most likely correspond to hydroxyl nitrates, nitrooxy hydroperoxides, and hydroxy hydroperoxy nitrates, respectively, but other constitutional isomers are possible. They were already observed in previous studies and were proposed to form through reactions of INO_2 radicals with RO_2, HO_2, and unimolecular rearrangement, as shown in Scheme S5 (Ng et al., 2008; Kwan et al., 2012; Schwantes et al., 2015; Wennberg et al., 2018).

As shown in Fig. 5b, the temporal evolution of $C_5H_9NO_7$ (*m/z* 274) is different to $C_5H_9NO_{4\text{-}6}$ compounds, suggesting that it has a completely different formation pathway. Specifically, the formation rate of $C_5H_9NO_7$ is initially much slower than that of $C_5H_9NO_{4\text{-}6}$ but accelerates to become comparable to them later as the experiment proceeds, i.e. when a multitude of first-generation products are accumulated. This implies that $C_5H_9NO_7$ is produced from the further oxidation of first-generation products, and its signal is dominated by second-generation products. Based on its molecular composition, $C_5H_9NO_7$ could be the dihydroperoxy nitrate as shown in Scheme S5, but its formation through the reaction of HO_2 with nitrooxy hydroperoxy radical from INO_2 autoxidation suggests it should be first-generation products, not in accordance with the time behavior we actually observe. Consequently, we can conclude that it is not the major formation pathway that contributed to $C_5H_9NO_7$ observed in this study. As shown in Scheme S7, the first-generation C_5 hydroxy carbonyl ($C_5H_8O_2$, *m/z* 179) can be further oxidized by NO_3 and the resulting alkyl radical would rapidly recombine with O_2, producing a new peroxy radical, which then reacts with HO_2 radicals to form $C_5H_9NO_7$ (hydroxy hydroperoxy carbonyl nitrate). Similarly, the C_5 hydroperoxy carbonyl ($C_5H_8O_3$, *m/z* 195) can also lead to the formation of such $C_5H_9NO_7$ (isomer of that formed through $C_5H_8O_2$ channel) through further oxidation (see Scheme S7). According to above two mechanisms, $C_5H_9NO_7$ formed following such reaction pathways should be second-generation products, better consistent with its time behavior.

Considering its similar time behavior to $C_5H_9NO_7$, the observed $C_4H_7NO_5$ (*m/z* 228) signal is likewise thought to be dominated by second-generation products. Schwantes et al. (2015) proposed such a C_4 product based on OH-initiated chemistry, but as the OH concentration in our system was below the detection limit during the experiment (see Fig. S2), this formation pathway cannot apply in our situation. Instead, we suggest that $C_4H_7NO_5$ is formed through the unimolecular decomposition of the C_5 alkoxy or acyl radicals, which result from further oxidation of the C_5 hydroxy carbonyl ($C_5H_8O_2$, *m/z* 179), as shown in Scheme S7. It should be pointed out here that there may be reaction pathways forming $C_4H_7NO_5$ as first-generation products that are not considered here, whereas it is no doubt that the second-generation chemistry played a dominant role in $C_4H_7NO_5$ formation according to its time evolution measured by CIMS.

Although $C_4H_7NO_5$ and $C_5H_9NO_7$ show similar time behaviors in the first three steps, it seems that they followed fairly different reaction pathways when the concentration of NO_3 in the chamber increased dramatically in step IV. As shown in Fig. 5b, the signal of $C_4H_7NO_5$ drops immediately after the injection of O_3 and NO_2, while that of $C_5H_9NO_7$ continues to increase, although its formation rate becomes slightly lower with increasing NO_3 concentration. The decay of $C_4H_7NO_5$ signal can be explained by more chemical destruction or less production under high NO_3 condition, wherein the latter seems more sensible in terms of its structure (no double bond remaining). As shown in Scheme S7, the second-generation $C_4H_7NO_5$ and $C_5H_9NO_7$ compounds share the same precursor in the $C_5H_8O_2$ channel. Consequently, the production of $C_5H_9NO_7$ through this pathway would be interrupted immediately after the injection of O_3 and NO_2 like $C_4H_7NO_5$. In reality, its signal might decay even faster due to the larger reaction rate of RO_2 H-shift (leading to the formation of $C_4H_7NO_5$) than that of RO_2 reacting with HO_2 (leading to the formation of $C_5H_9NO_7$). As presented by Vereecken and Nozière (2020), the rate coefficient of aldehydic H-shift is $\geq 0.5\ s^{-1}$ (298 K), while the pseudo first order rate coefficient of RO_2 reacting with HO_2 is $\sim 10^{-3}\ s^{-1}$ (k (298 K) = $5 \times 10^{-12}\ cm^3\ molecules^{-1} s^{-1}$ (Atkinson, 2007), and $[HO_2] \sim 4 \times 10^8$ molecules cm^{-3}), about two orders of magnitude smaller. This result implies that the increasing $C_5H_9NO_7$ observed is contributed to by other formation pathways. As mentioned before, $C_5H_9NO_7$ can also be produced by $C_5H_8O_3$ oxidation. We find that the signal of $C_4H_7NO_6$ (*m/z* 244), which results from $C_5H_8O_3$ oxidation as well, remains increasing after the injection of O_3 and NO_2. This tentatively confirms that the production of $C_5H_9NO_7$ in step IV is mainly from $C_5H_8O_3$ oxidation channel. More experimental or theoretical studies are needed to provide insights into these differences.

(2) 2N- and 3N-monomers

As shown in Fig. 5c, 2N-monomers formed much slower than 1N-monomers in the early stage, but their formation rates were accelerated in step II and step III, probably due to the accumulation of first-generation products. According to our mechanistic framework, 2N-monomers are second-generation products resulting from the further oxidation of 1N-monomers by NO_3, which is consistent with their time behaviors detected by CIMS.

Like $C_4H_7NO_5$ and $C_5H_9NO_7$, different 2N-monomers have similar behavior in the first three steps, but they are obviously different in step IV when the concentration of NO_3 increased drastically in the chamber. For instance, the signals of $C_5H_8N_2O_8$, $C_5H_8N_2O_9$ and $C_5H_{10}N_2O_8$ continue to increase after the injection of O_3 and NO_2, while that of $C_5H_{10}N_2O_9$ drops immediately. This is related to their detailed formation mechanisms which are outside the scope of this study. Furthermore, $C_5H_8N_2O_9$ and $C_5H_{10}N_2O_9$ decay a little bit faster than $C_5H_8N_2O_8$ and $C_5H_{10}N_2O_8$, which might be related to their volatility and will be further discussed in next section.

Different from other 2N-monomers, the signals of $C_5H_6N_2O_8$ (*m/z* 301) increases continuously under high NO_3 condition, although its net formation rate is almost zero at the end of step IV. The characteristics of $C_5H_6N_2O_8$ under high NO_3 condition reflects its different formation pathways from other dinitrates, and without having a comprehensive knowledge of its chemical mechanism, we are unable to tell what exactly leads to the differences. In the Master Chemical Mechanism (MCM v3.3.1), $C_5H_6N_2O_8$ is proposed to be a PAN-like compound stemming from the C_5 nitrooxy carbonyl ($C_5H_7NO_4$) (http://mcm.leeds.ac.uk/MCM/browse.htt?species=NC4CHO). Such $C_5H_6N_2O_8$ compound would react with NO_3 radicals due to the remaining double bond, and hence this cannot be the predominant formation pathway of the $C_5H_6N_2O_8$ observed in this study. Based on the formation mechanism of dinitrooxyepoxides ($C_5H_8N_2O_7$) proposed by Kwan et al. (2012), we suggest that $C_5H_6N_2O_8$ can also be a dinitrooxyepoxide resulting from cyclization of specific hydroperoxy alkyl radicals, as shown in Scheme S10. Alternatively, the C_5 hydroxy nitrate ($C_5H_9NO_4$) can be oxidized by NO_3 and then react with NO_3 radicals again, forming $C_5H_6N_2O_8$ with two aldehyde groups ultimately (see Scheme S10). According to the proposed mechanisms above, $C_5H_6N_2O_8$ formed through the first two pathways are second-generation products, while those from the third channel are third-generation products, in accordance with its time behavior measured by CIMS.

In addition to C_5-2N-monomers, we observe some C_4 dinitrates such as $C_4H_6N_2O_7$ (*m/z* 273) and $C_4H_8N_2O_8$ (*m/z* 291), and the signal intensity of $C_4H_6N_2O_7$ is comparable to the major C_5-2N-monomers. C_4 dinitrates have rarely been mentioned in previous isoprene-NO_3 studies. As shown in Fig. 5c, $C_4H_6N_2O_7$ has similar time behavior to C_5-2N-monomers, and hence is thought to be second-generation products. Wennberg et al. (2018) proposed that such a C4 dinitrate was generated from OH-initiated further oxidation of $C_5H_7NO_4$. However, this is not applicable here due to a lack of OH radicals in our system. Instead, we propose that the $C_4H_6N_2O_7$ observed in this study is dinitrooxy carbonyl compound resulting from NO_3 oxidation of $C_5H_7NO_4$ with subsequent unimolecular decomposition (see Scheme S11 for details).

As shown in Fig. 5d, 3N-monomers are generated more slowly than 1N-monomers, but their signals grow gradually as the experiment proceeds, with a significant increase especially for $C_5H_9N_3O_{10}$ in the last step. Furthermore, we can see from Fig. 5c and Fig. 5d that the signals of C_5 trinitrates in step IV appear anticorrelated to that of $C_5H_{10}N_2O_8$ and $C_5H_{10}N_2O_8$. The gas-phase 3N-monomers have rarely been reported in previous literature. Ng et al. (2008) observed $C_5H_9N_3O_{10}$ compound in the particle-phase and assumed that it was produced from NO_3 oxidation of the C_5 hydroxy nitrate ($C_5H_9NO_4$). Similarly, $C_5H_9N_3O_{11}$ and $C_5H_9N_3O_{12}$ can be formed through NO_3 reacting with dinitrooxy peroxy radicals, which result from corresponding first-generation nitrooxy compounds (C_5 hydroperoxy nitrate, $C_5H_9NO_5$ or C_5 hydroxy hydroperoxy nitrate, $C_5H_9NO_6$) oxidation by NO_3 radicals, as shown in Scheme S12. 3N-Monomers formed following such pathways are second-generation products by definition. Regarding the rising signals of 3N-monomers in step IV, one explanation is that although the reaction of dinitrooxy peroxy radicals with NO_3 is not an oxidation process, their formation can be significantly facilitated by increasing NO_3 concentration. It is also possible that 3N-monomers are formed through H-abstraction of 2N-monomers. NO_3 radicals can abstract the hydrogen of dihydroxy dinitrate ($C_5H_{10}N_2O_8$) or hydroxyl hydroperoxy dinitrate ($C_5H_{10}N_2O_9$) from the carbon with an –OH, –OOH or –ONO_2 group attached, leading to alkyl radicals that can subsequently recombine with O_2 and then react with NO_2 or NO_3, yielding trinitrates or peroxynitrates containing three nitrogen atoms. 3N-Monomers stemming from such reactions ought to be third-generation products. However, we should point out that 3N-monomers formed following H-abstraction pathway are less likely because abstracting hydrogen from the hydroxyl, hydroperoxy or nitrooxy carbon would lead to fragmentation at most cases (Bianchi et al., 2019).

In addition, it is interesting to note that the signal of $C_5H_9N_3O_{10}$ increases continuously throughout step IV, whereas that of $C_5H_9N_3O_{11}$and $C_5H_9N_3O_{12}$ drop after a short period of growth. Meanwhile, the production of $C_5H_9N_3O_{10}$ is facilitated by the increasing NO_3 concentration compared to that of $C_5H_9N_3O_{12}$ and $C_5H_9N_3O_{11}$. Currently, we cannot explain what exactly causes these differences, but we suspect that there may be different chemical pathways forming different 3N-monomers that are not covered here and may also be related to their different physical properties, such as vapor pressures.

(3) 2N- and 3N-dimers

As shown in Fig. 5e, 2N-dimers (except for $C_{10}H_{16}N_2O_{11}$) display very similar time behavior to 1N-monomer, which form rapidly after each injection, indicating that the signals of 2N-dimers are dominated by first-generation products like most 1N-monomers. It is noted that the time behavior of $C_{10}H_{16}N_2O_{11}$ (*m/z* 419) is completely different from that of other 2N-dimers. As illustrated in Fig. 5e, the production rate of $C_{10}H_{16}N_2O_{11}$ is initially much slower compared to other dimers. Besides, its signal increases monotonically in the first two oxidation stages, whereas that of the others always increase first, approaching the maximum as its chemical production competes against the losses, and decrease gradually thereafter. The special time behavior of $C_{10}H_{16}N_2O_{11}$ suggests that it has a different formation pathway from other 2N-dimers, and its signal is most likely dominated by secondary products. In addition, we find that the signal of $C_{10}H_{16}N_2O_{12}$ always starts to decay earlier than that of $C_{10}H_{16}N_2O_8$ and $C_{10}H_{16}N_2O_9$. If we assume that their production rates have the same order of magnitude (confirming by their formation rates after each injection), then it can be concluded that $C_{10}H_{16}N_2O_{12}$ had additional chemical destruction, or its volatility is much lower than $C_{10}H_{16}N_2O_8$ and $C_{10}H_{16}N_2O_9$ and hence has more rapid lost on the wall. It seems the second hypothesis is more likely when comparing its signal with and without dilution and wall-loss corrections (see Fig. S5). More detailed discussion about volatilities of different isoprene organonitrates will be provided in the next section.

It is proposed that dimers (ROOR') are likely formed through the self- or cross-reaction of two peroxy radicals (Berndt et al. 2018). Consequently, the generation number of dimers depends only on how the involved peroxy radicals are formed. Table S1 summarizes the possible permutation scheme of 2N-dimers from RO_2 + RO'_2 reactions, and their structural information can be found in Scheme S13. For example, self-reaction of two C_5 nitrooxy peroxy radicals ($C_5H_8NO_5$) leads to the formation of $C_{10}H_{16}N_2O_8$ compound, while recombination of two C_5 nitrooxy hydroxyl peroxy radicals ($C_5H_8NO_6$) or a C_5 nitrooxy peroxy radical ($C_5H_8NO_5$) with a C_5 nitrooxy hydroperoxy peroxy radical ($C_5H_8NO_7$) results in $C_{10}H_{16}N_2O_{10}$ compound. According to their time behavior, 2N-dimers (except for $C_{10}H_{16}N_2O_{11}$) are thought to be first-generation products, and from this fact we can infer that the peroxy radicals contributing to dimer formation are dominated by first-generation intermediates. With regard to $C_{10}H_{16}N_2O_{11}$, we conclude that it is most likely a secondary product considering its typical second-generation behavior. In other words, at least one of the two C_5 nitrooxy peroxy radicals involved in formation of $C_{10}H_{16}N_2O_{11}$ must be a secondary intermediate. As listed in Table S1, $C_{10}H_{16}N_2O_{11}$ can be formed through $C_5H_8NO_6$ + $C_5H_8NO_7$ or $C_5H_8NO_6$ + $C_5H_8NO_7$ reactions, wherein $C_5H_8NO_7$ and $C_5H_8NO_8$ would be secondary peroxy radicals if they are formed through NO_3 further oxidation of the C_5 hydroxy carbonyl compounds ($C_5H_8O_2$ or $C_5H_8O_3$), as shown in Scheme S7. In addition, it is possible that $C_{10}H_{16}N_2O_{11}$ is formed from a C_5 hydroxy peroxy radical $C_5H_9O_3$ reacting with a C_5 dinitrooxy hydroxy carbonyl peroxy radical $C_5H_7N_2O_{10}$ (from $C_5H_7NO_5$ oxidation by NO_3), as we observe high abundant $C_5H_{10}O_3$ during the experiment, although $C_5H_{10}O_3$ is assumed to be the major product of the OH-initiated chemistry.

Apart from 2N-dimers, we observe detectable signals at *m/z* 450, 466, 482, 498 and 514, which are identified as 3N-dimers with molecular formulas $C_{10}H_{17}N_3O_{12\text{-}16}$. $C_{10}H_{17}N_3O_{12}$ and $C_{10}H_{17}N_3O_{13}$ were detected in the particle-phase in previous study, suggesting that they have low volatility and can contribute to SOA formation (Ng et al., 2008). As shown in Fig. 5f, 3N-dimers form much slower than 2N-dimers, but their productions are accelerated as the experiment proceeds. This is similar to the characteristics of second-generation 2N- and 3N-monomers to some degree, suggesting that the signals of 3N-dimers we observed are most likely dominated by secondary or even later-generation compounds.

It is worth noting that $C_{10}H_{17}N_3O_{12\text{-}14}$ and $C_{10}H_{17}N_3O_{15,16}$ have two completely different types of time behavior. The signals of $C_{10}H_{17}N_3O_{12}$, $C_{10}H_{17}N_3O_{13}$ and $C_{10}H_{17}N_3O_{14}$ more or less increase in the first three oxidation steps and start to decline in the late of step III with increasing NO_3 concentration. As depicted in Scheme S13, 3N-dimers can result from further oxidation of 2N-dimers or the cross-reaction of a first-generation nitrooxy peroxy radical with a secondary dinitrooxy peroxy radical. Accordingly, such 3N-dimers are thought to be second-generation products, and they would further react with NO_3 due to the remaining double bond in their molecular structure, leading to severe chemical destruction of these compounds under high NO_3 condition. This is consistent with the time behavior of $C_{10}H_{17}N_3O_{12}$, $C_{10}H_{17}N_3O_{13}$ and $C_{10}H_{17}N_3O_{14}$. In contrast, $C_{10}H_{17}N_3O_{15}$ and $C_{10}H_{17}N_3O_{16}$ are formed even more slowly, and their production in the first four hours is close to zero. However, their signals start to climb in the late of step III, during which that of $C_{10}H_{17}N_3O_{12}$, $C_{10}H_{17}N_3O_{13}$ and $C_{10}H_{17}N_3O_{14}$ decline. This suggests that $C_{10}H_{17}N_3O_{15}$ and $C_{10}H_{17}N_3O_{16}$ formed under high NO_3 condition probably result from further reactions of $C_{10}H_{17}N_3O_{12\text{-}14}$. However, this assumption is highly uncertain and more experimental and theoretical studies are needed to substantiate it. In terms of their time behavior, $C_{10}H_{17}N_3O_{15}$ and $C_{10}H_{17}N_3O_{16}$ are thought to be third- or even later-generation products.

3.3 Volatility distribution of isoprene nitrates

3.3.1 C^* estimated by experimental methods

Detailed information about the volatility of organic molecules is essential to evaluate their potential to form SOA. In order to investigate the potential contribution of various isoprene oxidation products to SOA formation, we use our (limited) experimental data to estimate the vapor pressure of different isoprene organonitrates on the basis of their condensation behavior. Figure 6 shows how the signals of gas-phase products change in experiments with and without seed aerosols (ammonium sulfate). Please note that while the two experiments were conducted under similar conditions, the procedures could not be kept fully identical as aerosol seeding required specific measures and the oxidation chemistry might be slightly altered (e.g., due to initiation of heterogeneous reactions).

As shown in Fig. 6, the signals of most of the selected compounds decline when there are seed aerosols in the chamber, indicating that part of the condensable vapors is partitioned to the particle-phase due to the introduction of condensation sinks. The decrease in signal differs for different products, mostly depending on their vapor pressures. As expected, the lower volatility of a compound the higher the fraction that condenses. For instance, the signal of $C_5H_9NO_7$ decreases by more than 70% in experiment with seed aerosols, compared to less than 40% on average for other less-oxidized 1N-monomers. In some cases (e.g., $C_5H_9NO_4$ and $C_5H_9NO_5$) however, the product signals in experiment with seed aerosols are higher than that without seeds after the consumed isoprene exceeding a certain level. In addition, the signal of $C_5H_6N_2O_8$ in the experiment with seeds is always higher compared to that without seeds. One explanation for this phenomenon is the effect of heterogeneous reactions. It is likely that some condensed compound (denoted as A) can react on the particle surface to form new products with the molecular composition of compound B, or alternatively forming a precursor of B. When they evaporate back to the gas phase, it can result in an increase in signal of compound B. That's why a higher signal was observed for such compounds in experiment with seeds than that without seeds, as observed for $C_5H_6N_2O_8$ in this case.

Based on the observed condensation behavior of different products, we can derive their vapor pressures from the gas-particle equilibrium partitioning coefficients by Eq. (2). As depicted in Fig. 7, the saturation concentrations of different organonitrates show a decreasing tendency from 1N-, 2N-monomer and 3N-monomers to 2N- and 3N-dimers, suggesting that dimers have a higher propensity of condensation and contribute to SOA formation. This is partly related to their molecular weight, as larger molecules generally have lower vapor pressures. However, it cannot explain all the features of the volatility distribution. For example, $C_5H_9NO_6$ (corresponding to No.8 in Fig.7) has higher mass than $C_5H_9NO_5$ (corresponding to No.7 in Fig.7) but is predicted to have higher vapor pressure. In general, chemical composition and functionalities have significant effects on vapor pressure. For instance, the 2D-VBS composition-activity relationship suggests that each carbon and oxygen decrease C^* by 0.475 and 1.75 decades, respectively (Donahue et al., 2011). Different functional groups also have very different effect on volatility. For example, each hydroxyl group (–OH) or hydroperoxy group (–OOH) typically reduces the volatility by 2.4 to 2.5 decades, while the less polar carbonyl group (=O) reduces the volatility by 1 decade (Pankow and Asher 2008, Donahue et al., 2011). The nitrooxy group (–ONO_2) has a similar reductive effect on vapor pressure, which typically reduces C^* by 2.5 orders of magnitude (Pankow and Asher, 2008). Here, the irregularly high vapor pressure of $C_5H_9NO_6$ is most likely attributed to the functional groups it contains. As listed in Table S2, $C_5H_9NO_6$ is proposed to be nitrooxy hydroxy hydroperoxyl compound, which consists of two highly polar functional groups –OH and –OOH, contributing to formation of intramolecular H-bonding that can significantly increase the vapor pressure (Bilde et al., 2015; Kurten et al., 2016), while $C_5H_9NO_5$ only contains a –OOH group and hence cannot form intramolecular H-bonding. This explanation is also valid for $C_5H_9N_3O_{10}$ and $C_5H_9N_3O_{12}$. In summary, these findings underline that the constitutional and configurational information of a molecule is critical for vapor-pressure estimation.

3.3.2 C^* estimated by different parametrization methods

For comparison, we also adopt different parameterization methods to estimate the saturation vapor pressures of isoprene oxidation products based on their molecular composition and the proposed structures, with the results depicted in Fig. 7. In general, the saturation concentrations calculated by different parameterization methods show a similar volatility distribution to that calculated by experimental method, with C^* of 1N-, 2N- and 3N-monomers, 2N- and 3N-dimers decreasing in turn. However, different parameterization methods lead to the predicted vapor concentrations with a variability of several orders of magnitude for the same compound, and the discrepancies become larger and larger with more complicated molecules. In addition, C^* of structural isomers calculated by the same method could span several decades.

As shown in Fig. 7, the Donahue et al. parameterization mostly provides lower C^* compared to the three GC methods, with a maximum discrepancy up to 12 orders of magnitude for dimers. With regard to smaller and less oxidized 1N-monomers, predicted C^* values from different methods are in relatively good agreement with each other, whereas the disagreement increases to 11 orders of magnitude for 2N- and 3N-monomers. This is mainly the case because the organic molecules were regarded as a mixture of =O and –OH functional groups in the Donahue et al. parameterization, and their relative abundance was assumed to be 1:1 (Donahue et al., 2011). In consequence, the –OOH functional group in peroxides is treated as two –OH groups when adapting the method proposed by Donahue et al. (2011). However, it is demonstrated that the extra oxygen in peroxy moieties has little contribution to reduce vapor pressure (Pankow and Asher et al., 2008), hence treating –OOH equivalent to two –OH functional groups would underestimate the vapor pressures of hydroperoxyl compounds. Furthermore, organic compounds consisting of multiple polar functional groups (such as hydroperoxy, peroxy acid, and peroxide functional groups) tend to form intramolecular H-bonding, which would increase the vapor pressure (Bilde et al., 2015; Kurten et al., 2016). All these issues contribute to an underestimation of the vapor pressures of multifunctional products when using the Donahue et al. parameterization. Mohr et al. (2019) improved the parameterization for vapor-pressure estimation by taking the presence of –OOH functional groups in HOM explicitly into consideration and revising the parameters to reduce the effect of –OOH on depressing C^*. Consequently, the Mohr et al. parameterization effectively reduces the discrepancy between its estimates and those predicted by the GC methods, with the differences within 6 orders of magnitude. Nevertheless, there is a slight tendency to underestimate the vapor pressures of 3N-monomers and dimers. The Peräkylä et al. parameterization method, which was derived from measurements of the condensation behavior of HOM produced from α-pinene ozonolysis, predicts similar C^* to Donahue et al. method for 1N-monomers, but higher C^* for 2N- and 3N-monomers like the Mohr et al. method. As for dimers, especially for the 3N-dimers containing more multifunctional groups, the Peräkylä et al. method even predicts higher C^* than the GC methods in most cases.

Three GC methods predict similar saturation vapor pressures for different isoprene nitrates in this work, with the differences within 5 orders of magnitudes. Generally, the SIMPOL.1 method always provides higher C^* compared to another two methods, and the disagreement between methods becomes larger for molecules containing multifunctional groups. For instance, the vapor-pressure discrepancy between SIMPOL.1 and another two GC methods are both 2 orders of magnitude for $C_5H_9NO_{4,5}$ and $C_{10}H_{17}N_3O_{12-14}$, but it increased up to 4 and 5 orders of magnitude, respectively, for $C_5H_9NO_{6,7}$ and $C_{10}H_{17}N_3O_{15,16}$.

It is worth noting that the Nannoolal et al. method is able to distinguish between positional isomers (e.g., the estimated C^* for two $C_5H_{10}N_2O_9$ isomers are 0.858 and 0.333 μg m^{-3}, respectively), whereas such capacity of EVAPORATION method is limited (e.g., it is able to distinguish between the position isomers of $C_5H_{10}N_2O_9$, but it predicts identical C^* for $C_{10}H_{16}N_2O_{11}$ isomers). In this respect, the SIMPOL.1 method cannot distinguish between positional isomers at all. Moreover, SIMPOL.1 method predicts smaller differences between functional group isomers for 1N-monomers and 3N-dimers compared to the Nannoolal et al. method and the EVAPORATION, but there is no such regular pattern for 2N-monomers and 2N-dimers.

By comparing the results calculated by experimental method with those by different parameterization methods, we can see that the GC methods predict high saturation concentrations for 1N-monomers than the experimental method, while the Donahue et al. and Peräkylä et al. method provide similar C^* values. With regard to 2N-monomers, the GC methods predict higher vapor pressures compared to the experimental method, but the discrepancy decreases with decreasing saturation concentration. The disagreement of C^* for 2N-monomers estimated by experimental method and the Mohr et al. or Peräkylä et al. method are within 2 orders of magnitude. In terms of low-volatility dimers, however, the vapor pressures calculated by the experimental method were 1–3 orders of magnitude larger than that predicted by the parameterization methods except for the Peräkylä et al. method. The Peräkylä et al. method provides the most similar predictions to the experimental method for isoprene oxidation products in the full volatility range, with the disagreement within 1 order of magnitude.

In general, the vapor pressures estimated experimentally in this study are very close to that calculated by Peräkylä et al. method for which the estimation parameters were also derived experimentally. The discrepancy between the experimental and the GC methods spans several orders of magnitude depending on different compounds, with the GC methods predicting higher C^* for less-functionalized 1N-monomers, approximate C^* for 2N-monomers, but lower C^* for highly functionalized dimers. It is difficult to tell which method is more reliable without any measured saturation vapor pressure data on such multifunctional organic nitrates. However, considering the fact that the existing GC methods tend to underestimate saturation vapor pressures of the highly functionalized organic molecules due to their limited capability to deal with intramolecular interactions (e.g. the intramolecular hydrogen bonding formed among polar functional groups), and the well consistent results of two experimentally derived methods, we suggest that the experimental method might be a good choice to determine the volatility of highly oxidized compounds accurately.

3.3.3 Volatility distribution of isoprene nitrates and expected SOA yields.

Although the vapor pressures calculated by different methods show a variability of several orders of magnitude, the predicted volatility distributions of different organic groups are consistent. To eliminate the discrepancy caused by methods and get an average trend of the volatility distribution of various isoprene nitrates, we use the median value of C^* calculated by different methods as the estimator of the vapor pressure for each nitrate compound.

The average carbon oxidation state is plotted against $Log_{10}(C^*)$ in Fig. 8 to describe the volatility distribution of organic nitrates formed from isoprene oxidation by NO_3. Generally, the volatility of measured gas-phase products spans a wide range from IVOC to ELVOC, wherein all of the 1N-monomers fall in the IVOC or SVOC range, suggesting that 1N-monomers have low potential to form SOA by simple condensation as long as the organic aerosol load is less than 200 μg m^{-3}. The addition of a second or third –NO_3 functional group decreases C^* of most 2N- and 3N-monomers by 2-3 decades compared with 1N-monomers, and most of them belong to SVOC. They will start to condense in significant fractions if the organic aerosol load is in a range of 1-10 μg m^{-3}, which means 2N- and 3N-monomers with $OS_c > -0.8$ may contribute to SOA formation under atmospheric conditions. With regard to dimers, all 3N-dimers and 2N-dimers (except for $C_{10}H_{16}N_2O_{8,9}$) are in LVOC or even ELVOC range, indicating isoprene dimers had high propensity to form SOA even at organic aerosol loads << 1 μg/m^3. However, we would like to emphasize here that the signals of 2N- and 3N-dimers only account for less than 2% on average of the total assigned signals, as shown in Fig. S6. This suggests that the SOA yield of isoprene from NO_3 oxidation by condensation should be low under atmospheric conditions.

The fate of RO_2 determines the product distribution directly and hence could substantially affect SOA yields and aerosol physicochemical properties (Boyd et al., 2015; Fry et al., 2018; Ng et al., 2008; Schwantes et al., 2015; Ziemann and Atkinson, 2012). Consequently, it would be helpful to provide SOA yields together with the fate of RO_2. In our experiment, reactions with HO_2 and NO_3 the dominant loss channels for the initially formed RO_2 from isoprene oxidation by NO_3, contributing for ~ 53% and ~ 30% of overall RO_2 loss; RO_2 + RO_2 reactions contributed a minor fraction (~ 13%) followed by unimolecular reactions with a contribution of ~ 5%, according to modelling results (Brownwood et al., 2021). More details about the modelling and the results can be found elsewhere (Brownwood et al., 2021; Vereecken et al., 2021).

In polluted urban regions, the fate of RO_2 is typically dominated by RO_2 + NO_3, while in the more pristine environment, the RO_2 + HO_2 reaction will dominate RO_2 fate (Bianchi et al., 2019; Boyd et al., 2015; Brown and Stutz, 2012). RO_2 + HO_2 was more important in the chamber than that in ambient and enhanced RO_2 + HO_2 would potentially lead to less dimer formation by RO_2 + RO_2 reactions and hence reducing SOA yields. However, a recent work from Brownwood et al. (2021) based on the same campaign as this study pointed out that the bulk aerosol composition and SOA yields were largely independent of RO_2 fate. Similarly, Boyd et al. (2015) found for β-pinene-NO_3 system that RO_2 fate ("RO_2 + NO_3 dominant" vs "RO_2 + HO_2 dominant") had only few effects on SOA formation. Therefore, the SOA yield estimated in this study is expected to be comparable to that in the atmosphere.

Assuming that the dimers in the LVOC or ELVOC range will condense onto particles, we estimated a SOA mass yield for condensation of isoprene organic nitrates of about 5 % ± 2 %. This value is based on an averaged bulk organonitrate sensitivity of 0.019 norm. count s^{-1} $ppbv^{-1}$ and has been corrected for wall loss and dilution (see Fig. S7, with uncorrected SOA mass yield of about 2 %). The estimated SOA mass yield is within the range of those reported in the literature, but at the lower end (4.3% to 23.8% depending on RO_2 fate, Ng et al., 2008; 0.7% for first generation oxidation and 14% after oxidation of both double bonds, Rollins et al., 2009; 27% on average for ambient measurements, Fry et al., 2018). The SOA yield will probably become somewhat higher if taking the contribution of SVOCs (including $C_{10}H_{16}N_2O_8$, $C_{10}H_{16}N_2O_9$ and some other monomers, as shown in Fig. 8) into consideration. Our finding is commensurable with the SOA yield for isoprene organic nitrates of 2-6% derived from HR-AMS measurements in the same campaign (Brownwood et al., 2021).

In addition, Br^- adduct ionization CIMS is selective for HO_2 and less oxidized organic compounds (Albrecht et al., 2019; Rissanen et al., 2019), so it is reasonable to assume that there were more highly oxidized products that were not detected by Br^- CIMS. This assumption is confirmed by measurements with a NO_3^- CIMS performed in another isoprene-NO_3 experiment in SAPHIR (Zhao et al., 2021). Zhao et al. (2021) observed a higher fraction of dimers and more highly oxidized monomers and dimers, as well as trimers (C_{15} compounds). As a consequence, the SOA yields derived from NO_3^- CIMS measurements is slightly higher.

From these points of view our yield is more a lower limit. However, even if we assume an error of a factor of 2, the SOA yield of isoprene organic nitrates by condensation is more likely in a range of about 10% or less than in the higher range of 20-30% published in the literature. Of course, by our method we cannot cover any liquid phase processes that would lead to additional SOA beyond the condensation of the target compounds.

4. Conclusions and implication

In this work, a gas-phase experiment conducted in the SAPHIR chamber under near atmospheric conditions in the dark was analyzed to primarily investigate the multi-generation chemistry of isoprene-NO_3 system. The characteristics of a diversity of isoprene nitrates were measured by the CIMS using Br^- as the reagent ion. Isoprene 1N-, 2N-, and 3N-monomers and 2N- and 3N-dimers have different time behaviors, indicating the occurrence of multi-generation oxidation during this process. Based on their specific time behaviors as well as the general knowledge of isoprene and radical chemistry, the possible formation mechanisms of these compounds are proposed.

In order to evaluate the potential contribution of various isoprene nitrates to SOA formation, different composition-activity and group-contribution methods were used to estimate their saturation vapor pressures. We also calculated the vapor pressures of isoprene oxidation products based on the gas-particle equilibrium coefficients derived from condensation measurements. The vapor pressures estimated by different methods spans several orders of magnitude, and the discrepancies increase as the compounds become highly functionalized. It shows that existing composition-activity methods (especially the Donahue et al. method) seriously underestimate the saturation vapor pressure of multifunctional low-volatility molecules compared to the experimental methods The group-contribution methods seem to have a better performance than the CA methods on this aspect, but they still have a tendency to underestimate the vapor pressures of multifunctional molecules. We suggest that experimental methods is a good choice to estimate the volatility of highly oxidized compounds accurately.

According to our results, 1N-monomers and most 2N and 3N-nitrates fall in the IVOC or SVOC range. Therefore, they have, with a few exceptions, low potential to form SOA at atmospheric organic aerosol loads. In contrast, 2N- and 3N-dimers are estimated to have low or extremely low volatility, indicating that they are significant contributors to SOA formation, although dimers constitute less than 2% of the total explained signals. In this study, no new particle formation events were observed. Assuming that the dimers in the LVOC or ELVOC range will condense onto particles completely, we estimate a SOA mass yield of about 5 % ± 2 %, which is a lower limit if one takes a possible contribution of the minor dimer products as well as SVOC species into consideration. Both the volatility distribution and calculated SOA yields indicate that isoprene dimers formed from NO_3 oxidation are the major contributors to SOA formation.

Data availability

All data given in figures can be displayed in tables or in digital form. This includes the data given in the Supplement. Please send all requests for data to t.mentel@fz-juelich.de and r.wu@fz-juelich.de.

The data used in this work are available on the EUROCHAMP data base (https://data.eurochamp.org/data-access/chamber-experiments/, EUROCHAMP, 2020) under https://doi.org/10.25326/JTYK-5V47 and https://doi.org/10.25326/0SPZ-BN30.

Author contributions

HF, JNC, JLF, SSB, AW, and AKS designed the study. Instrument deployment and data analysis were carried out by RW, ET, SK, SRA, LH, AN, HF, RT, TH, PTMC, JS, FB, BB, JAT. RW, LV, ET, DZ, JAT, MH, TFM interpreted the compiled data set. RW, TFM, LV wrote the manuscript. All co-authors discussed the results and commented on the manuscript.

Competing interests

The authors declare that they have no conflict of interest.

Acknowledgements

This work has received funding from the European Research Council (ERC) and European Commission (EC) under the European Union's Horizon 2020 research and innovation program (SARLEP grant agreement No. 681529, Eurochamp 2020 grant agreement No. 730997 and FORCeS, grant No.821205). R.Wu gratefully acknowledges the fellowship from Helmholtz-OCPC (Office of China Postdoc Council) Postdoc Program for research support. M. Hallquist, E. Tsiligiannis and Th. F. Mentel acknowledge support by the Swedish Research Council (grant numbers 2014-05332 and 2018-04430) and FORMAS (grant numbers 2015-1537 and 2019-586).

References

Albrecht, S. R., Novelli, A., Hofzumahaus, A., Kang, S., Baker, Y., Mentel, T., Wahner, A., and Fuchs, H.: Measurements of hydroperoxy radicals (HO2) at atmospheric concentrations using bromide chemical ionisation mass spectrometry, Atmos. Meas. Tech., 12, 891-902, 10.5194/amt-12-891-2019, 2019.

Anglada, J. M., Crehuet, R., and Francisco, J. S.: The Stability of α-Hydroperoxyalkyl Radicals, Chem. Eur. J., 22, 18092-18100, 2016.

Atkinson, R., and Arey, J.: Gas-phase tropospheric chemistry of biogenic volatile organic compounds: a review, Atmos. Environ., 37, 197-219, 10.1016/S1352-2310(03)00391-1, 2003.

Atkinson, R.: Gas-phase tropospheric chemistry of organic compounds: a review, Atmos. Environ., 41, 200-240, 10.1016/j.atmosenv.2007.10.068, 2007.

Barber, V. P., Pandit, S., Green, A. M., Trongsiriwat, N., Walsh, P. J., Klippenstein, S. J., and Lester, M. I.: Four-carbon Criegee intermediate from isoprene ozonolysis: Methyl vinyl ketone oxide synthesis, infrared spectrum, and OH production, J. Am. Chem. Soc., 140, 10866-10880, 2018.

Berndt, T., Mentler, B., Scholz, W., Fischer, L., Herrmann, H., Kulmala, M., and Hansel, A.: Accretion Product Formation from Ozonolysis and OH Radical Reaction of alpha-Pinene: Mechanistic Insight and the Influence of Isoprene and Ethylene, Environ. Sci. Technol., 52, 11069-11077, 10.1021/acs.est.8b02210, 2018.

Bianchi, F., Kurten, T., Riva, M., Mohr, C., Rissanen, M. P., Roldin, P., Berndt, T., Crounse, J. D., Wennberg, P. O., Mentel, T. F., Wildt, J., Junninen, H., Jokinen, T., Kulmala, M., Worsnop, D. R., Thornton, J. A., Donahue, N., Kjaergaard, H. G., and Ehn, M.: Highly Oxygenated Organic Molecules (HOM) from Gas-

Phase Autoxidation Involving Peroxy Radicals: A Key Contributor to Atmospheric Aerosol, Chem. Rev., 119, 3472-3509, 10.1021/acs.chemrev.8b00395, 2019.

Bilde, M., Barsanti, K., Booth, M., Cappa, C. D., Donahue, N. M., Emanuelsson, E. U., McFiggans, G., Krieger, U. K., Marcolli, C., Topping, D., Ziemann, P., Barley, M., Clegg, S., Dennis-Smither, B., Hallquist, M., Hallquist, A. M., Khlystov, A., Kulmala, M., Mogensen, D., Percival, C. J., Pope, F., Reid, J. P., Ribeiro da Silva, M. A., Rosenoern, T., Salo, K., Soonsin, V. P., Yli-Juuti, T., Prisle, N. L., Pagels, J., Rarey, J., Zardini, A. A., and Riipinen, I.: Saturation vapor pressures and transition enthalpies of low-volatility organic molecules of atmospheric relevance: from dicarboxylic acids to complex mixtures, Chem. Rev., 115, 4115-4156, 10.1021/cr5005502, 2015.

Brown, S., Degouw, J., Warneke, C., Ryerson, T., Dubé, W., Atlas, E., Weber, R., Peltier, R., Neuman, J., and Roberts, J.: Nocturnal isoprene oxidation over the Northeast United States in summer and its impact on reactive nitrogen partitioning and secondary organic aerosol, Atmos. Chem. Phys., 9, 3027-3042, 10.5194/acp-9-3027-2009, 2009.

Brown, S. S., and Stutz, J.: Nighttime radical observations and chemistry, Chem. Soc. Rev., 41, 6405-6447, 2012.

Brownwood, B., Turdziladze, A., Hohaus, T., Wu, R., Mentel, T. F., Carlsson, P. T., Tsiligiannis, E., Hallquist, M., Andres, S., and Hantschke, L.: Gas-particle partitioning and SOA yields of organonitrate products from NO3-initiated oxidation of isoprene under varied chemical regimes, ACS Earth Space Chem., 2021.

Boyd, C., Sanchez, J., Xu, L., Eugene, A. J., Nah, T., Tuet, W., Guzman, M. I., and Ng, N.: Secondary organic aerosol formation from the β-pinene+ NO 3 system: effect of humidity and peroxy radical fate, Atmos. Chem. Phys., 15, 7497-7522, 2015.

Carlton, A. G., Wiedinmyer, C., and Kroll, J. H.: A review of Secondary Organic Aerosol (SOA) formation from isoprene, Atmos. Chem. Phys., 9, 4987-5005, 10.5194/acp-9-4987-2009, 2009.

Compernolle, S., Ceulemans, K., and Müller, J. F.: EVAPORATION: a new vapour pressure estimation methodfor organic molecules including non-additivity and intramolecular interactions, Atmos. Chem. Phys., 11, 9431-9450, 10.5194/acp-11-9431-2011, 2011.

Crosson, E.: A cavity ring-down analyzer for measuring atmospheric levels of methane, carbon dioxide, and water vapor, Appl. Phys. B, 92, 403-408, 10.1007/s00340-008-3135-y, 2008.

Crounse, J. D., Nielsen, L. B., Jørgensen, S., Kjaergaard, H. G., and Wennberg, P. O.: Autoxidation of Organic Compounds in the Atmosphere, J. Phys. Chem. Lett., 4, 3513-3520, 10.1021/jz4019207, 2013.

Dommen, J., Hellen, H., Saurer, M., Jaeggi, M., Siegwolf, R., Metzger, A., Duplissy, J., Fierz, M., and Baltensperger, U.: Determination of the aerosol yield of isoprene in the presence of an organic seed with carbon isotope analysis, Environ. Sci. Technol., 43, 6697-6702, 2009.

Donahue, N. M., Robinson, A. L., Stanier, C. O., and Pandis, S. N.: Coupled partitioning, dilution, and chemical aging of semivolatile organics, Environ. Sci. Technol., 40, 2635-2643, 10.1021/es052297c, 2006.

Donahue, N. M., Epstein, S. A., Pandis, S. N., and Robinson, A. L.: A two-dimensional volatility basis set: 1. organic-aerosol mixing thermodynamics, Atmos. Chem. Phys., 11, 3303-3318, 10.5194/acp-11-3303-2011, 2011.

Donahue, N. M., Kroll, J. H., Pandis, S. N., and Robinson, A. L.: A two-dimensional volatility basis set – Part 2: Diagnostics of organic-aerosol evolution, Atmos. Chem. Phys., 12, 615-634, 10.5194/acp-12-615-2012, 2012.

Dubé, W. P., Brown, S. S., Osthoff, H. D., Nunley, M. R., Ciciora, S. J., Paris, M. W., McLaughlin, R. J., and Ravishankara, A.: Aircraft instrument for simultaneous, in situ measurement of NO 3 and N 2 O 5 via pulsed cavity ring-down spectroscopy, Rev. Sci. Instrum., 77, 034101, 10.1063/1.2176058, 2006.

Ehn, M., Thornton, J. A., Kleist, E., Sipila, M., Junninen, H., Pullinen, I., Springer, M., Rubach, F., Tillmann, R., Lee, B., Lopez-Hilfiker, F., Andres, S., Acir, I. H., Rissanen, M., Jokinen, T., Schobesberger, S., Kangasluoma, J., Kontkanen, J., Nieminen, T., Kurten, T., Nielsen, L. B., Jorgensen, S., Kjaergaard, H. G., Canagaratna, M., Maso, M. D., Berndt, T., Petaja, T., Wahner, A., Kerminen, V. M., Kulmala, M., Worsnop, D. R., Wildt, J., and Mentel, T. F.: A large source of low-volatility secondary organic aerosol, Nature, 506, 476-479, 10.1038/nature13032, 2014.

Friedman, B., and Farmer, D. K.: SOA and gas phase organic acid yields from the sequential photooxidation of seven monoterpenes, Atmos. Environ., 187, 335-345, 10.1016/j.atmosenv.2018.06.003, 2018.

Fry, J. L., Brown, S. S., Middlebrook, A. M., Edwards, P. M., Campuzano-Jost, P., Day, D. A., Jimenez, J. L., Allen, H. M., Ryerson, T. B., Pollack, I., Graus, M., Warneke, C., de Gouw, J. A., Brock, C. A., Gilman, J., Lerner, B. M., Dubé, W. P., Liao, J., and Welti, A.: Secondary organic aerosol (SOA) yields from NO₃ radical + isoprene based on nighttime aircraft power plant plume transects, Atmos. Chem. Phys., 18, 11663-11682, 10.5194/acp-18-11663-2018, 2018.

Guenther, A., Jiang, X., Heald, C., Sakulyanontvittaya, T., Duhl, T., Emmons, L., and Wang, X.: The Model of Emissions of Gases and Aerosols from Nature version 2.1 (MEGAN2. 1): an extended and updated framework for modeling biogenic emissions, Geosci. Model Dev., 5, 1471–1492, 10.5194/gmd-5-1471-2012, 2012. .

Hallquist, M., Wenger, J., Baltensperger, U., Rudich, Y., Simpson, D., Claeys, M., Dommen, J., Donahue, N., George, C., and Goldstein, A.: The formation, properties and impact of secondary organic aerosol: current and emerging issues, Atmos. Chem. Phys., 9, 5155–5236, 10.5194/acp-9-5155-2009, 2009 .

Hu, J., Wu, L., Zheng, B., Zhang, Q., He, K., Chang, Q., Li, X., Yang, F., Ying, Q., and Zhang, H.: Source contributions and regional transport of primary particulate matter in China, Environ. Pollut., 207, 31-42, 10.1016/j.envpol.2015.08.037, 2015.

Jenkin, M. E., Valorso, R., Aumont, B., and Rickard, A. R.: Estimation of rate coefficients and branching ratios for reactions of organic peroxy radicals for use in automated mechanism construction, Atmos. Chem. Phys., 19, 7691–7717, https://doi.org/10.5194/acp-19-7691-2019, 2019.

Jenkin, M., Young, J., and Rickard, A.: The MCM v3. 3.1 degradation scheme for isoprene, Atmos. Chem. Phys., 15, 11433–11459, 10.5194/acp-15-11433-2015, 2015.

Jimenez, J. L., Canagaratna, M., Donahue, N., Prevot, A., Zhang, Q., Kroll, J. H., DeCarlo, P. F., Allan, J. D., Coe, H., and Ng, N.: Evolution of organic aerosols in the atmosphere, science, 326, 1525-1529, 10.1126/science.1180353, 2009.

Kim, P. S., Jacob, D. J., Fisher, J. A., Travis, K., Yu, K., Zhu, L., Yantosca, R. M., Sulprizio, M. P., Jimenez, J. L., Campuzano-Jost, P., Froyd, K. D., Liao, J., Hair, J. W., Fenn, M. A., Butler, C. F., Wagner, N. L., Gordon, T. D., Welti, A., Wennberg, P. O., Crounse, J. D., St. Clair, J. M., Teng, A. P., Millet, D. B., Schwarz, J. P., Markovic, M. Z., and Perring, A. E.: Sources, seasonality, and trends of southeast US aerosol: an integrated analysis of surface, aircraft, and satellite observations with the GEOS-Chem chemical transport model, Atmos. Chem. Phys., 15, 10411-10433, 10.5194/acp-15-10411-2015, 2015.

Kirkby, J., Duplissy, J., Sengupta, K., Frege, C., Gordon, H., Williamson, C., Heinritzi, M., Simon, M., Yan, C., Almeida, J., Trostl, J., Nieminen, T., Ortega, I. K., Wagner, R., Adamov, A., Amorim, A., Bernhammer, A. K., Bianchi, F., Breitenlechner, M., Brilke, S., Chen, X., Craven, J., Dias, A., Ehrhart, S., Flagan, R. C., Franchin, A., Fuchs, C., Guida, R., Hakala, J., Hoyle, C. R., Jokinen, T., Junninen, H., Kangasluoma, J., Kim, J., Krapf, M., Kurten, A., Laaksonen, A., Lehtipalo, K., Makhmutov, V., Mathot, S., Molteni, U., Onnela, A., Perakyla, O., Piel, F., Petaja, T., Praplan, A. P., Pringle, K., Rap, A., Richards, N. A., Riipinen, I., Rissanen, M. P., Rondo, L., Sarnela, N., Schobesberger, S., Scott, C. E., Seinfeld, J. H., Sipila, M., Steiner, G., Stozhkov, Y., Stratmann, F., Tome, A., Virtanen, A., Vogel, A. L., Wagner, A. C., Wagner, P. E., Weingartner, E., Wimmer, D., Winkler, P. M., Ye, P., Zhang, X., Hansel, A., Dommen, J., Donahue, N. M., Worsnop, D. R., Baltensperger, U., Kulmala, M., Carslaw, K. S., and Curtius, J.: Ion-induced nucleation of pure biogenic particles, Nature, 533, 521-526, 10.1038/nature17953, 2016.

Kleindienst, T. E., Lewandowski, M., Offenberg, J. H., Jaoui, M., and Edney, E. O.: Ozone-isoprene reaction: Re-examination of the formation of secondary organic aerosol, Geophys. Res. Lett., 34, 10.1029/2006GL027485, 2007.

Krechmer, J., Lopez-Hilfiker, F., Koss, A., Hutterli, M., Stoermer, C., Deming, B., Kimmel, J., Warneke, C., Holzinger, R., Jayne, J., Worsnop, D., Fuhrer, K., Gonin, M., and de Gouw, J.: Evaluation of a New Reagent-Ion Source and Focusing Ion-Molecule Reactor for Use in Proton-Transfer-Reaction Mass Spectrometry, Anal. Chem., 90, 12011-12018, 10.1021/acs.analchem.8b02641, 2018.

Kroll, J. H., Ng, N. L., Murphy, S. M., Flagan, R. C., and Seinfeld, J. H.: Secondary organic aerosol formation from isoprene photooxidation, Environ. Sci. Technol., 40, 1869-1877, 10.1021/es0524301, 2006.

Kroll, J. H., Donahue, N. M., Jimenez, J. L., Kessler, S. H., Canagaratna, M. R., Wilson, K. R., Altieri, K. E., Mazzoleni, L. R., Wozniak, A. S., Bluhm, H., Mysak, E. R., Smith, J. D., Kolb, C. E., and Worsnop, D. R.: Carbon oxidation state as a metric for describing the chemistry of atmospheric organic aerosol, Nat. Chem., 3, 133-139, 10.1038/nchem.948, 2011.

Kurten, T., Tiusanen, K., Roldin, P., Rissanen, M., Luy, J.-N., Boy, M., Ehn, M., and Donahue, N.: α-Pinene autoxidation products may not have extremely low saturation vapor pressures despite high O: C ratios, J. Phys. Chem. A, 120, 2569-2582, 10.1021/acs.jpca.6b02196, 2016.

Kwan, A., Chan, A., Ng, N., Kjærgaard, H. G., Seinfeld, J., and Wennberg, P.: Peroxy radical chemistry and OH radical production during the NO3-initiated oxidation of isoprene, Atmos. Chem. Phys., 12, 7499–7515, 10.5194/acp-12-7499-2012, 2012.

Marais, E. A., Jacob, D. J., Jimenez, J. L., Campuzano-Jost, P., Day, D. A., Hu, W., Krechmer, J., Zhu, L., Kim, P. S., Miller, C. C., Fisher, J. A., Travis, K., Yu, K., Hanisco, T. F., Wolfe, G. M., Arkinson, H. L., Pye, H. O. T., Froyd, K. D., Liao, J., and McNeill, V. F.: Aqueous-phase mechanism for secondary organic aerosol formation from isoprene: application to the southeast United States and co-benefit of SO2 emission controls, Atmos. Chem. Phys., 16, 1603-1618, 10.5194/acp-16-1603-2016, 2016.

McFiggans, G., Mentel, T. F., Wildt, J. r., Pullinen, I., Kang, S., Kleist, E., Schmitt, S., Springer, M., Tillmann, R., Wu, C., Zhao, D., Hallquist, M., Faxon, C., Le Breton, M., Hallquist, A. s. M., Simpson, D., Bergström, R., Jenkin, M. E., Ehn, M., Thornton, J. A., Alfarra, M. R., Bannan, T. J., Percival, C. J., Priestley, M., Topping, D., and Kiendler-Scharr, A.: Secondary organic aerosol reduced by mixture of atmospheric vapours, Nature, 565, 587-593, 10.1038/s41586-018-0871-y, 2019.

Mentel, T. F., Springer, M., Ehn, M., Kleist, E., Pullinen, I., Kurtén, T., Rissanen, M., Wahner, A., and Wildt, J.: Formation of highly oxidized multifunctional compounds: autoxidation of peroxy radicals formed in the ozonolysis of alkenes – deduced from structure–product relationships, Atmos. Chem. Phys., 15, 6745-6765, 10.5194/acp-15-6745-2015, 2015.

Mohr, C., Thornton, J. A., Heitto, A., Lopez-Hilfiker, F. D., Lutz, A., Riipinen, I., Hong, J., Donahue, N. M., Hallquist, M., Petaja, T., Kulmala, M., and Yli-Juuti, T.: Molecular identification of organic vapors driving atmospheric nanoparticle growth, Nat. Commun., 10, 4442, 10.1038/s41467-019-12473-2, 2019.

Molteni, U., Simon, M., Heinritzi, M., Hoyle, C. R., Bernhammer, A.-K., Bianchi, F., Breitenlechner, M., Brilke, S., Dias, A., Duplissy, J., Frege, C., Gordon, H., Heyn, C., Jokinen, T., Kürten, A., Lehtipalo, K., Makhmutov, V., Petäjä, T., Pieber, S. M., Praplan, A. P., Schobesberger, S., Steiner, G., Stozhkov, Y., Tomé, A., Tröstl, J., Wagner, A. C., Wagner, R., Williamson, C., Yan, C., Baltensperger, U., Curtius, J., Donahue, N. M., Hansel, A., Kirkby, J., Kulmala, M., Worsnop, D. R., and Dommen, J.: Formation of Highly Oxygenated Organic Molecules from α-Pinene Ozonolysis: Chemical Characteristics, Mechanism, and Kinetic Model Development, ACS Earth Space Chem., 3, 873-883, 10.1021/acsearthspacechem.9b00035, 2019.

Mutzel, A., Rodigast, M., Iinuma, Y., Böge, O., and Herrmann, H.: Monoterpene SOA – Contribution of first-generation oxidation products to formation and chemical composition, Atmos. Environ., 130, 136-144, 10.1016/j.atmosenv.2015.10.080, 2016.

Nannoolal, Y., Rarey, J., Ramjugernath, D., and Cordes, W.: Estimation of pure component properties: Part 1. Estimation of the normal boiling point of non-electrolyte organic compounds via group contributions and group interactions, Fluid Phase Equilib., 226, 45-63, 10.1016/j.fluid.2004.09.001, 2004.

Nannoolal, Y., Rarey, J., and Ramjugernath, D.: Estimation of pure component properties: Part 3. Estimation of the vapor pressure of non-electrolyte organic compounds via group contributions and group interactions, Fluid Phase Equilib., 269, 117-133, 10.1016/j.fluid.2008.04.020, 2008.

Ng, N., Kwan, A., Surratt, J., Chan, A., Chhabra, P., Sorooshian, A., Pye, H. O., Crounse, J., Wennberg, P., and Flagan, R.: Secondary organic aerosol (SOA) formation from reaction of isoprene with nitrate radicals (NO3), Atmos. Chem. Phys., 8, 4117–4140, 10.5194/acp-8-4117-2008, 2008.

Ng, N. L., Chhabra, P. S., Chan, A. W. H., Surratt, J. D., Kroll, J. H., Kwan, A. J., McCabe, D. C., Wennberg, P. O., Sorooshian, A., Murphy, S. M., Dalleska, N. F., Flagan, R. C., and Seinfeld, J. H.: Effect of NO_x level on secondary organic aerosol (SOA) formation from the photooxidation of terpenes, Atmos. Chem. Phys., 7, 5159-5174, 10.5194/acp-7-5159-2007, 2007.

Ng, N. L., Brown, S. S., Archibald, A. T., Atlas, E., Cohen, R. C., Crowley, J. N., Day, D. A., Donahue, N. M., Fry, J. L., Fuchs, H., Griffin, R. J., Guzman, M. I., Herrmann, H., Hodzic, A., Iinuma, Y., Jimenez, J. L., Kiendler-Scharr, A., Lee, B. H., Luecken, D. J., Mao, J., McLaren, R., Mutzel, A., Osthoff, H. D., Ouyang, B., Picquet-Varrault, B., Platt, U., Pye, H. O. T., Rudich, Y., Schwantes, R. H., Shiraiwa, M., Stutz, J., Thornton, J. A., Tilgner, A., Williams, B. J., and Zaveri, R. A.: Nitrate radicals and biogenic volatile organic compounds: oxidation, mechanisms, and organic aerosol, Atmos. Chem. Phys., 17, 2103-2162, 10.5194/acp-17-2103-2017, 2017.

Novelli, A., Cho, C., Fuchs, H., Hofzumahaus, A., Rohrer, F., Tillmann, R., Kiendler-Scharr, A., Wahner, A., and Vereecken, L.: Experimental and theoretical study on the impact of a nitrate group on the chemistry of alkoxy radicals, Phys. Chem. Chem. Phys., 23, 5474–5495, https://doi.org/10.1039/d0cp05555g, 2021.

Novelli, A., Vereecken, L., Bohn, B., Dorn, H.-P., Gkatzelis, G. I., Hofzumahaus, A., Holland, F., Reimer, D., Rohrer, F., and Rosanka, S.: Importance of isomerization reactions for OH radical regeneration from the photo-oxidation of isoprene investigated in the atmospheric simulation chamber SAPHIR, Atmos. Chem. Phys., 20, 3333–3355, 10.5194/acp-20-3333-2020, 2020.

O'Meara, S., Booth, A. M., Barley, M. H., Topping, D., and McFiggans, G.: An assessment of vapour pressure estimation methods, Phys. Chem. Chem. Phys., 16, 19453-19469, 10.1039/c4cp00857j, 2014.

Orlando, J. J., Tyndall, G. S., and Wallington, T. J.: The atmospheric chemistry of alkoxy radicals, Chem. Rev., 103, 4657-4690, 10.1021/cr020527p, 2003.

Orlando, J. J., and Tyndall, G. S.: Laboratory studies of organic peroxy radical chemistry: an overview with emphasis on recent issues of atmospheric significance, Chem. Soc. Rev., 41, 6294-6317, 10.1039/C2CS35166H, 2012.

Pankow, J. F., and Asher, W. E.: SIMPOL.1: a simple group contribution method for predicting vapor pressures and enthalpies of vaporization of multifunctional organic compounds, Atmos. Chem. Phys., 8, 2773-2796, 10.5194/acp-8-2773-2008, 2008.

Peeters, J., Müller, J.-F. o., Stavrakou, T., and Nguyen, V. S.: Hydroxyl radical recycling in isoprene oxidation driven by hydrogen bonding and hydrogen tunneling: The upgraded LIM1 mechanism, J. Phys. Chem. A, 118, 8625-8643, 10.1021/jp5033146, 2014.

Peräkylä, O., Riva, M., Heikkinen, L., Quéléver, L., Roldin, P., and Ehn, M.: Experimental investigation into the volatilities of highly oxygenated organic molecules (HOM), Atmos. Chem. Phys., 20, 649–669, 10.5194/acp-20-649-2020, 2020.

Pöschl, U.: Atmospheric aerosols: composition, transformation, climate and health effects, Angew. Chem. Int. Ed., 44, 7520-7540, 10.1002/anie.200501122, 2005.

Praske, E., Otkjær, R. V., Crounse, J. D., Hethcox, J. C., Stoltz, B. M., Kjaergaard, H. G., and Wennberg, P. O.: Atmospheric autoxidation is increasingly important in urban and suburban North America, Proc. Natl. Acad. Sci. U.S.A., 115, 64-69, 10.1073/pnas.1715540115, 2018.

Rissanen, M. P., Kurten, T., Sipila, M., Thornton, J. A., Kangasluoma, J., Sarnela, N., Junninen, H., Jorgensen, S., Schallhart, S., Kajos, M. K., Taipale, R., Springer, M., Mentel, T. F., Ruuskanen, T., Petaja, T., Worsnop, D. R., Kjaergaard, H. G., and Ehn, M.: The formation of highly oxidized multifunctional products in the ozonolysis of cyclohexene, J. Am. Chem. Soc., 136, 15596-15606, 10.1021/ja507146s, 2014.

Rissanen, M. P., Mikkilä, J., Iyer, S., and Hakala, J.: Multi-scheme chemical ionization inlet (MION) for fast switching of reagent ion chemistry in atmospheric pressure chemical ionization mass spectrometry (CIMS) applications, Atmos. Meas. Tech., 12, 6635–6646, 10.5194/amt-12-6635-2019, 2019.

Riva, M., Rantala, P., Krechmer, J. E., Peräkylä, O., Zhang, Y., Heikkinen, L., Garmash, O., Yan, C., Kulmala, M., Worsnop, D., and Ehn, M.: Evaluating the performance of five different chemical ionization techniques for detecting gaseous oxygenated organic species, Atmos. Meas. Tech., 12, 2403-2421, 10.5194/amt-12-2403-2019, 2019.

Rohrer, F., Bohn, B., Brauers, T., Brüning, D., Johnen, F. J., Wahner, A., and Kleffmann, J.: Characterisation of the photolytic HONO-source in the atmosphere simulation chamber SAPHIR, Atmos. Chem. Phys., 5, 2189-2201, 10.5194/acp-5-2189-2005, 2005.

Rollins, A. W., Kiendler-Scharr, A., Fry, J., Brauers, T., Brown, S. S., Dorn, H.-P., Dubé, W. P., Fuchs, H., Mensah, A., and Mentel, T.: Isoprene oxidation by nitrate radical: alkyl nitrate and secondary organic aerosol yields, Atmos. Chem. Phys., 9, 6685–6703, 10.5194/acp-9-6685-2009, 2009.

Schwantes, R. H., Teng, A. P., Nguyen, T. B., Coggon, M. M., Crounse, J. D., St Clair, J. M., Zhang, X., Schilling, K. A., Seinfeld, J. H., and Wennberg, P. O.: Isoprene NO3 Oxidation Products from the RO2 + HO2 Pathway, J. Phys. Chem. A, 119, 10158-10171, 10.1021/acs.jpca.5b06355, 2015.

Schwantes, R. H., Charan, S. M., Bates, K. H., Huang, Y., Nguyen, T. B., Mai, H., Kong, W., Flagan, R. C., and Seinfeld, J. H.: Low-volatility compounds contribute significantly to isoprene secondary organic aerosol (SOA) under high-NO_{<i>x</i>} conditions, Atmos. Chem. Phys., 19, 7255-7278, 10.5194/acp-19-7255-2019, 2019.

Sobanski, N., Schuladen, J., Schuster, G., Lelieveld, J., and Crowley, J. N.: A five-channel cavity ring-down spectrometer for the detection of NO2, NO3, N2O5, total peroxy nitrates and total alkyl nitrates, Atmos. Meas. Tech., 9, 5103–5118, 10.5194/amt-9-5103-2016, 2016.

Spracklen, D., Jimenez, J., Carslaw, K., Worsnop, D., Evans, M., Mann, G., Zhang, Q., Canagaratna, M., Allan, J., and Coe, H.: Aerosol mass spectrometer constraint on the global secondary organic aerosol budget, Atmos. Chem. Phys., 11, 12109–12136, 10.5194/acp-11-12109-2011, 2011.

Stadtler, S., Kühn, T., Schröder, S., Taraborrelli, D., Schultz, M. G., and Kokkola, H.: Isoprene-derived secondary organic aerosol in the global aerosol–chemistry–climate model ECHAM6.3.0–HAM2.3–MOZ1.0, Geosci. Model Dev., 11, 3235-3260, 10.5194/gmd-11-3235-2018, 2018.

Starn, T., Shepson, P., Bertman, S., Riemer, D., Zika, R., and Olszyna, K.: Nighttime isoprene chemistry at an urban‐impacted forest site, J. Geophys. Res. Atmos., 103, 22437-22447, 1998.

Stroud, C., Roberts, J., Williams, E., Hereid, D., Angevine, W., Fehsenfeld, F., Wisthaler, A., Hansel, A., Martinez‐Harder, M., and Harder, H.: Nighttime isoprene trends at an urban forested site during the 1999 Southern Oxidant Study, J. Geophys. Res. Atmos., 107, ACH 7-1-ACH 7-14, 2002.

Suh, I., Lei, W., and Zhang, R.: Experimental and Theoretical Studies of Isoprene Reaction with NO3, J. Phys. Chem. A, 105, 6471-6478, 10.1021/jp0105950, 2001.

Surratt, J. D., Chan, A. W., Eddingsaas, N. C., Chan, M., Loza, C. L., Kwan, A. J., Hersey, S. P., Flagan, R. C., Wennberg, P. O., and Seinfeld, J. H.: Reactive intermediates revealed in secondary organic aerosol formation from isoprene, Proc. Natl. Acad. Sci. U.S.A., 107, 6640-6645, 10.1073/pnas.0911114107, 2010.

Thornton, J. A., Shilling, J. E., Shrivastava, M., D'Ambro, E. L., Zawadowicz, M. A., and Liu, J.: A Near-Explicit Mechanistic Evaluation of Isoprene Photochemical Secondary Organic Aerosol Formation and Evolution: Simulations of Multiple Chamber Experiments with and without Added NOx, ACS Earth Space Chem., 10.1021/acsearthspacechem.0c00118, 2020.

Tröstl, J., Chuang, W. K., Gordon, H., Heinritzi, M., Yan, C., Molteni, U., Ahlm, L., Frege, C., Bianchi, F., and Wagner, R.: The role of low-volatility organic compounds in initial particle growth in the atmosphere, Nature, 533, 527-531, 10.1038/nature18271, 2016.

Vereecken, L., Nguyen, T. L., Hermans, I., and Peeters, J.: Computational study of the stability of α-hydroperoxyl-or α-alkylperoxyl substituted alkyl radicals, Chem. Phys. Lett., 393, 432-436, 10.1016/j.cplett.2004.06.076, 2004.

Vereecken, L.: Computational study of the stability of α-nitroxy-substituted alkyl radicals, Chem. Phys. Lett., 466, 127-130, 10.1016/j.cplett.2008.10.042, 2008.

Vereecken, L., and Peeters, J.: Decomposition of substituted alkoxy radicals—part I: a generalized structure–activity relationship for reaction barrier heights, Phys. Chem. Chem. Phys., 11, 9062-9074, 10.1039/B909712K, 2009.

Vereecken, L., and Peeters, J.: A structure–activity relationship for the rate coefficient of H-migration in substituted alkoxy radicals, Phys. Chem. Chem. Phys., 12, 12608-12620, 10.1039/C0CP00387E, 2010.

Vereecken, L., and Francisco, J. S.: Theoretical studies of atmospheric reaction mechanisms in the troposphere, Chem. Soc. Rev., 41, 6259-6293, 10.1039/C2CS35070J, 2012.

Vereecken, L., and Nozière, B.: H migration in peroxy radicals under atmospheric conditions, Atmos. Chem. Phys., 20, 7429-7458, 10.5194/acp-20-7429-2020, 2020.

Vereecken, L., Carlsson, P., Novelli, A., Bernard, F., Brown, S. S., Cho, C., Crowley, J. N., Fuchs, H., Mellouki, W., Reimer, D., Shenolikar, Justin, Tillmann, R., Zhou, L., Kiendler-Scharr, A., and Wahner, A.: Theoretical and experimental study of peroxy and alkoxy radicals in the NO_3-initiated oxidation of isoprene, Phys. Chem. Chem. Phys., 23, 5496–5515, https://doi.org/10.1039/d0cp06267g, 2021.

Wang, S., Riva, M., Yan, C., Ehn, M., and Wang, L.: Primary formation of highly oxidized multifunctional products in the OH-Initiated oxidation of Isoprene: a combined theoretical and experimental study, Environ. Sci. Technol., 52, 12255-12264, 10.1021/acs.est.8b02783, 2018.

Warneke, C., De Gouw, J., Goldan, P., Kuster, W., Williams, E., Lerner, B., Jakoubek, R., Brown, S., Stark, H., and Aldener, M.: Comparison of daytime and nighttime oxidation of biogenic and anthropogenic VOCs along the New England coast in summer during New England Air Quality Study 2002, J. Geophys. Res. Atmos., 109, 2004.

Wennberg, P. O., Bates, K. H., Crounse, J. D., Dodson, L. G., McVay, R. C., Mertens, L. A., Nguyen, T. B., Praske, E., Schwantes, R. H., and Smarte, M. D.: Gas-phase reactions of isoprene and its major oxidation products, Chem. Rev., 118, 3337-3390, 10.1021/acs.chemrev.7b00439, 2018.

Whalley, L., Stone, D., and Heard, D.: New insights into the tropospheric oxidation of isoprene: combining field measurements, laboratory studies, chemical modelling and quantum theory, in: Atmospheric and Aerosol Chemistry, edited by: McNeill, V. F., and Ariya, P. A., Springer, Berlin, Heidelberg, Germany, 55-95, 10.1007/128_2012_359, 2012.

Zhang, Q., Jimenez, J. L., Canagaratna, M., Allan, J., Coe, H., Ulbrich, I., Alfarra, M., Takami, A., Middlebrook, A., and Sun, Y.: Ubiquity and dominance of oxygenated species in organic aerosols in anthropogenically‐influenced Northern Hemisphere midlatitudes, Geophys. Res. Lett., 34, 10.1029/2007GL029979, 2007.

Zhao, D., Pullinen, I., Fuchs, H., Schrade, S., Wu, R., Acir, I.-H., Tillmann, R., Rohrer, F., Wildt, J., and Guo, Y.: Highly oxygenated organic molecules (HOM) formation in the isoprene oxidation by NO3 radical, Atmos. Chem. Phys. Discuss., 1-28, 2020.

Ziemann, P. J., and Atkinson, R.: Kinetics, products, and mechanisms of secondary organic aerosol formation, Chem. Soc. Rev., 41, 6582-6605, 10.1039/c2cs35122f, 2012.

1275

Tables

Table 1: Summary of estimation methods of saturation vapor pressure used in this study

Estimation method	Methodology	Input information			Reference
		molecular formula	functional groups	others	
Donahue et al.	CA[a]	√			Donahue et al., 2011
Mohr et al.	ICA[b]	√			Mohr et al., 2019
Peräkylä et al.	ICA[b]	√			Peräkylä et al., 2020
Nannoolal et al.	GC[c]	√	√	√ [d]	Nannoolal et al., 2008
SIMPOL.1	GC	√	√		Pankow and Asher, 2008
EVAPORATION	GC	√	√		Compernolle et al., 2011
This study	EXP[e]				

[a] abbreviation of composition-activity method; [b] abbreviation of improved composition-activity method, which modified the parameterization based on chamber measurements to better fit HOMs; [c] abbreviation of group-contribution method; [d] boiling point parameterization method is also required to be defined; [e] abbreviation of experimental method.

Figures

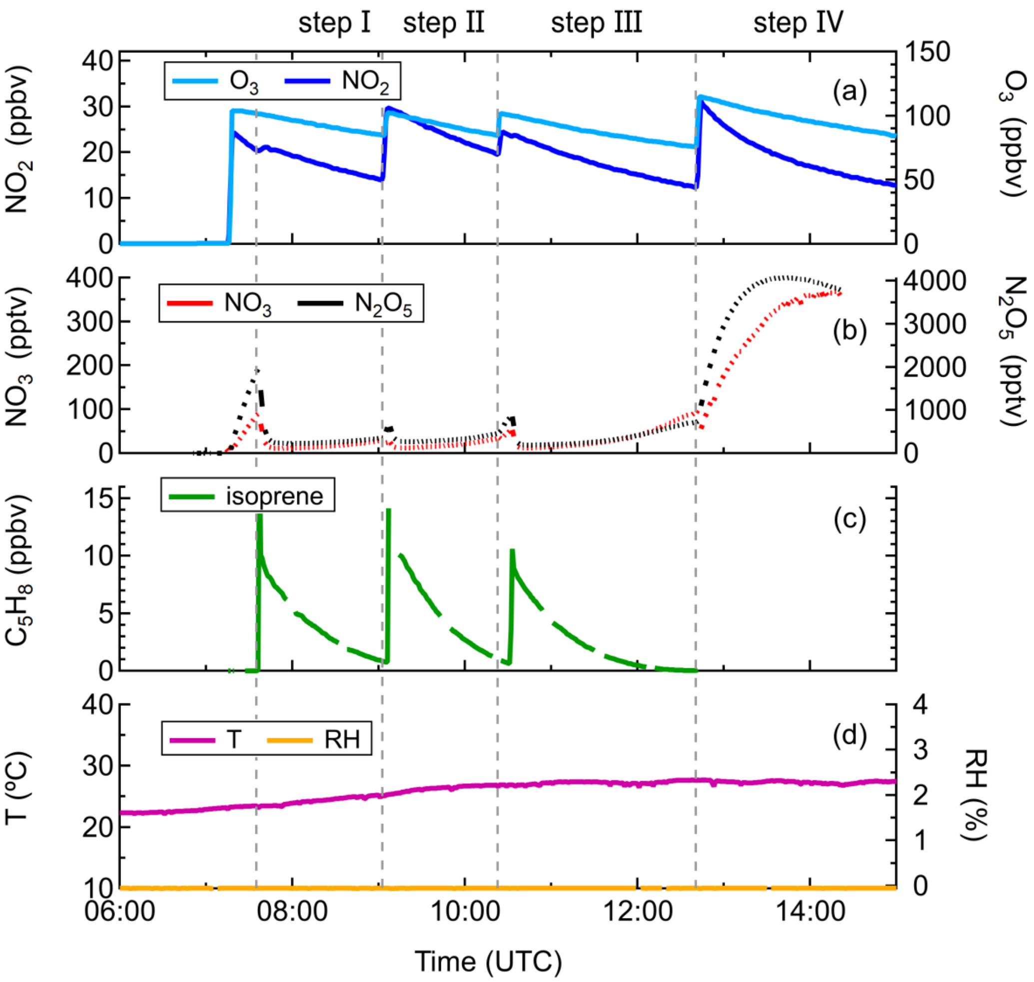

Figure 1: Measurements of (A) O_3 and NO_2, (B) NO_3 and N_2O_5, (C) isoprene and (D) temperature and relative humidity in the chamber during the experiment on 08 August, 2018.

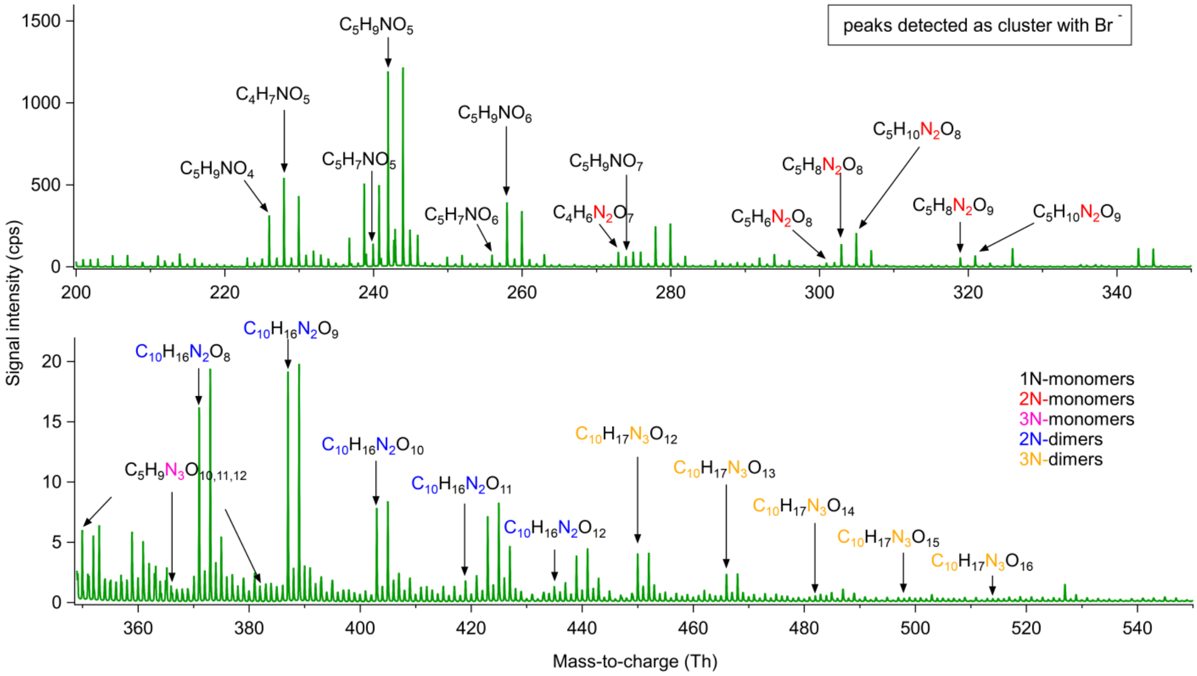

Figure 2: Averaged mass spectra for isoprene-NO_3 experiment on 8 August, 2018. Molecular formulas were determined according to the accurate mass data provided by HR-ToF-CIMS.

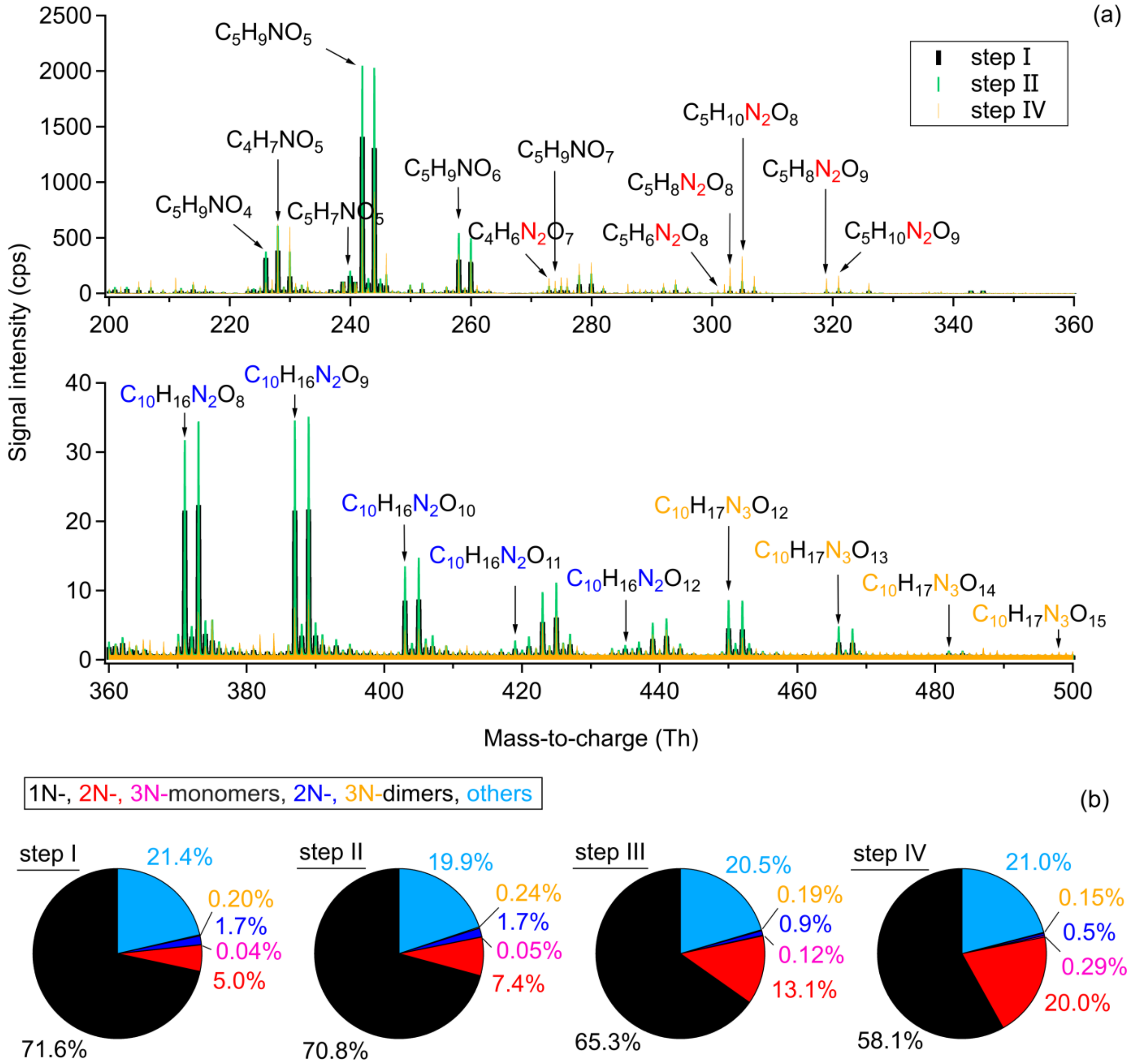

Figure 3: Comparison of the chemical composition of each oxidation step. (A) Averaged mass spectra for step I, II, and IV, with the omitted spectrum of step III being very similar to that of step II. (B) Relative contribution of different chemical groups for each oxidation step. Only organic products were counted for analysis. 'Others' refers to CHO compounds without containing nitrogen atoms (e.g., $C_5H_8O_2$ and $C_5H_8O_3$).

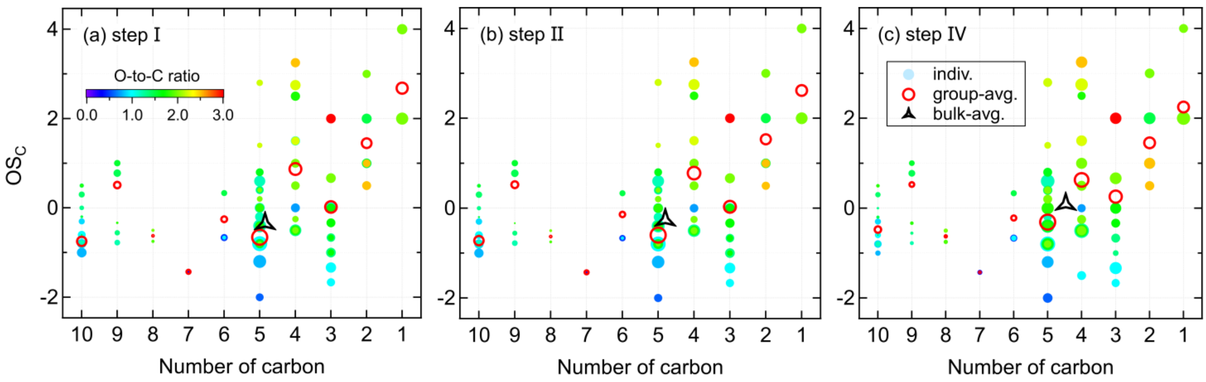

Figure 4: Distribution of gas-phase products from isoprene oxidation by NO_3 in the carbon oxidation state (*OS_C*) versus carbon number (*n_C*) space. Markers are colored by oxygen-to-carbon molar ratio and sized by the logarithm of peak areas. The group-averaged and bulk-averaged $\overline{OS_C}$ are signal-weighted mean average carbon oxidation state of compounds with the same carbon number and of all detected compounds, respectively.

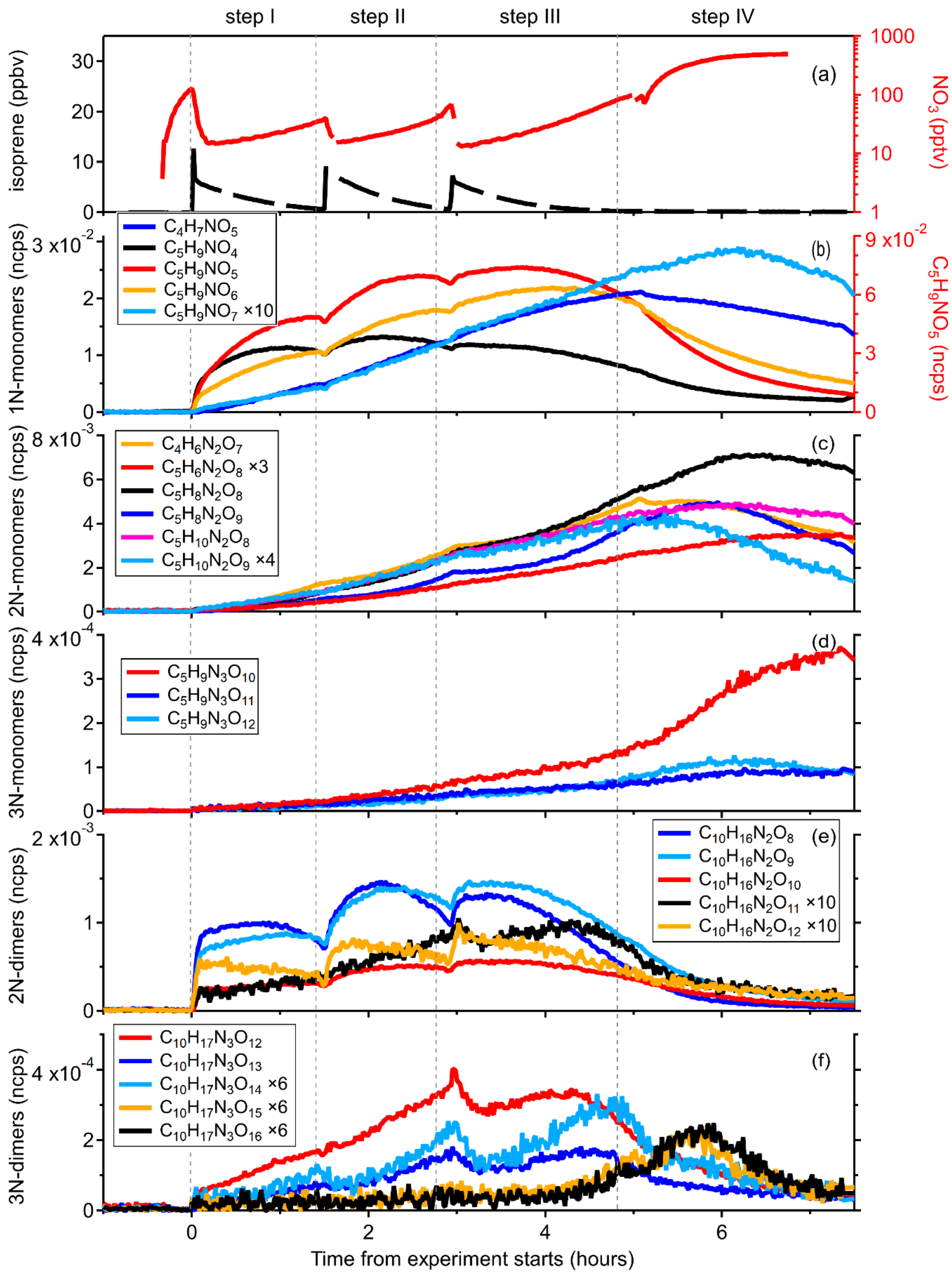

Figure 5: Time evolution of selected gas-phase compounds measured during the isoprene - NO_3 experiment on 08 August, 2018. (a) Time series of O_3, NO_2, NO_3 and isoprene. (b)–(f) Time evolution of major 1N-monomers ($C_5H_9NO_{4-7}$ and $C_4H_7NO_5$), 2N-monomers ($C_4H_6N_2O_7$, $C_5H_6N_2O_8$, and $C_5H_{8,10}N_2O_{8,9}$), 3N-monomers ($C_5H_9N_3O_{10-12}$), 2N-dimers ($C_{10}H_{16}N_2O_{8-12}$), and 3N-dimers ($C_{10}H_{17}N_3O_{12-16}$).

1323

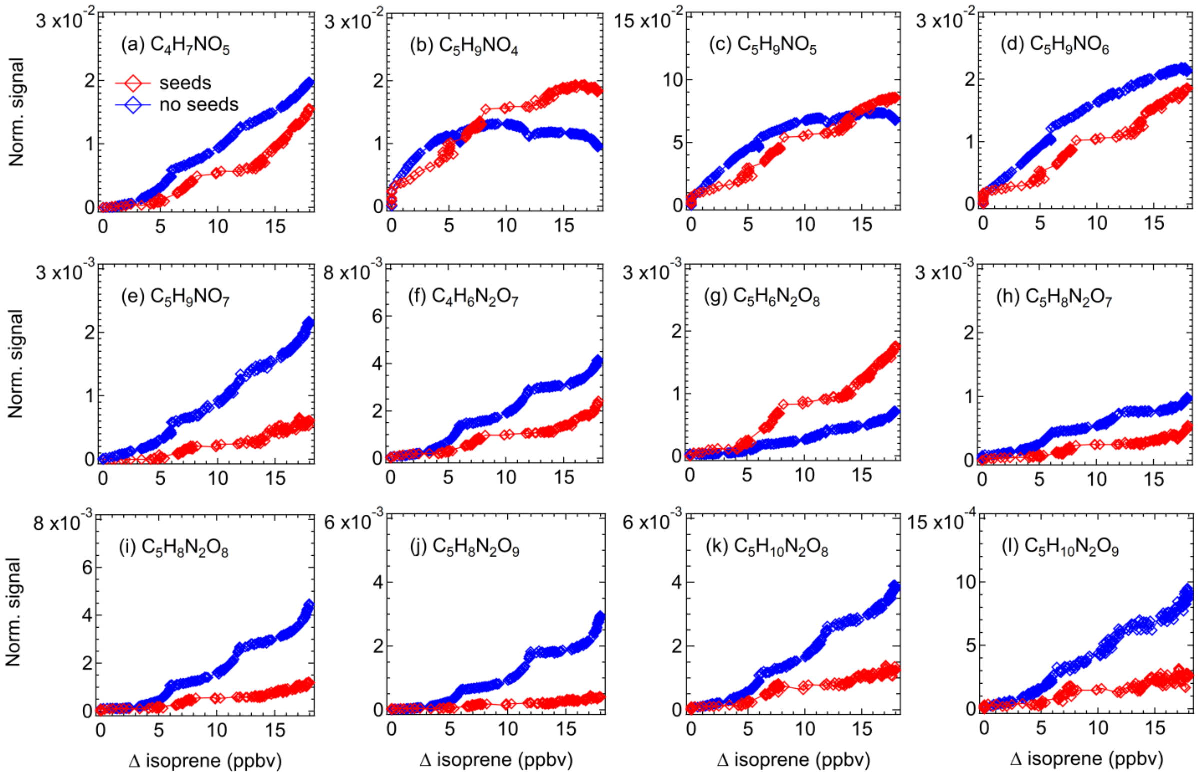

Figure 6: Time evolution of selected major gas-phase products during experiments with (red) and without (blue) seed aerosols (ammonium sulfate). Signals have been corrected for dilution.

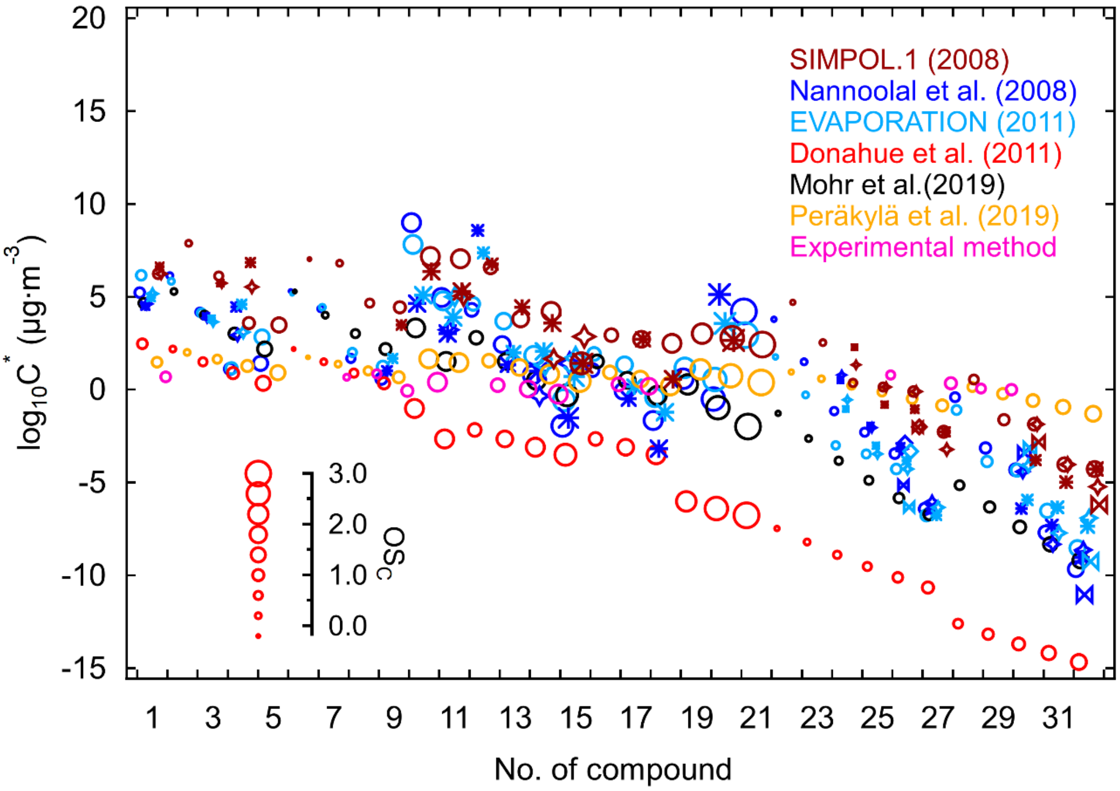

Figure 7: Saturation concentrations (in μg m^{-3}, at 298.15 K) of isoprene organonitrates estimated by using experimental and parameterization methods. The numbers correspond with the compound numbers of given in Table S2 (No. 1–9, 10–18, 19–21, 22–27, and 28–32 corresponding to 1N-monomers, 2N-monomers, 3N-monomer, 2N-dimers and 3N-dimers, respectively). Marker shapes indicate different isomers, with their size scaled by carbon oxidation state (*OS$_C$*).

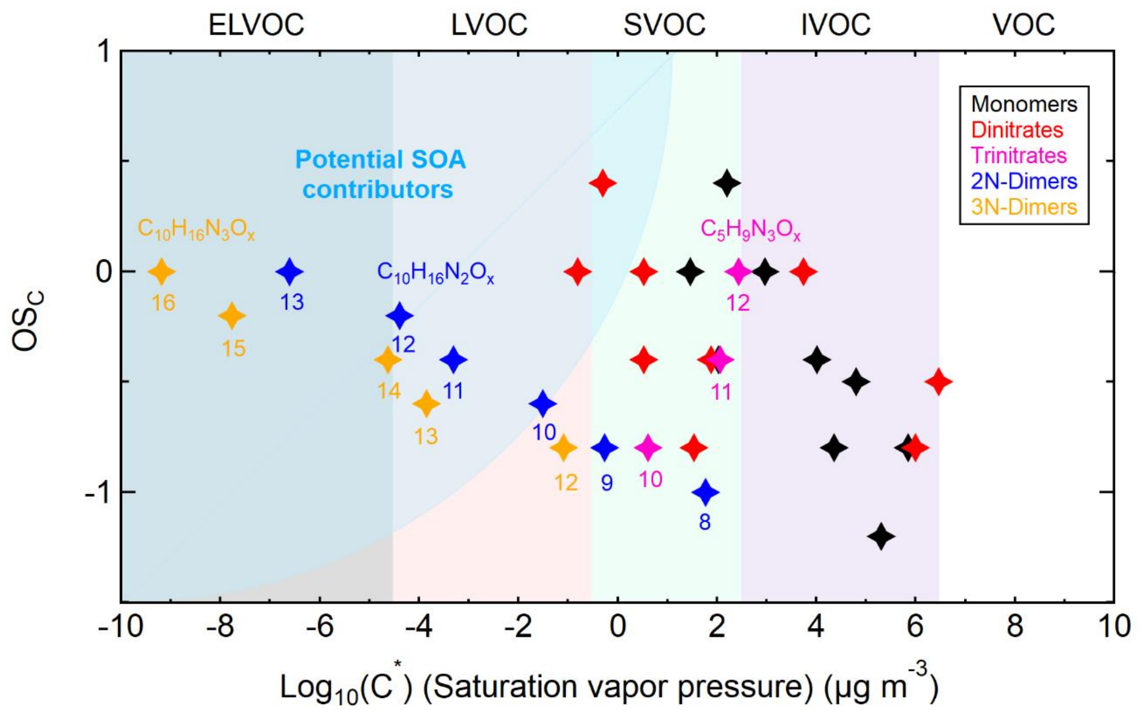

Figure 8: Volatility distribution of different organonitrates formed from NO_3-initiated isoprene oxidation. The volatility classes are indicated along the top with corresponding colors in the plot. The position of potential SOA contributors is determined depending on the exact functionalities of molecules adapted from Bianchi et al. (2019).